

MASARYKOVA UNIVERZITA
PŘÍRODOVĚDECKÁ FAKULTA
ÚSTAV TEORETICKÉ FYZIKY A ASTROFYZIKY

Diplomová práce

BRNO 2016

ROMANA GROSSOVÁ



MASARYKOVA UNIVERZITA
PŘÍRODOVĚDECKÁ FAKULTA
ÚSTAV TEORETICKÉ FYZIKY A ASTROFYZIKY



Vysokodisperzní spektroskopie s Ondřejovským Ešeletovým Spektrografem

Diplomová práce

Romana Grossová

Vedoucí práce: RNDr. Petr Škoda, CSc. Brno 2016

Bibliografický záznam

Autor: Bc. Romana Grossová
Přírodovědecká fakulta, Masarykova univerzita
Ústav teoretické fyziky a astrofyziky

Název práce: Vysokodisperzní spektroskopie s Ondřejovským Ešeletovým
Spektrografem

Studijní program: Fyzika

Studijní obor: Teoretická fyzika a astrofyzika

Vedoucí práce: RNDr. Petr Škoda, CSc.

Akademický rok: 2015/2016

Počet stran: viii + 68

Klíčová slova: Ešeletový spektrograf, IRAF, OPERA, exoplanety

Bibliographic Entry

Author: Bc. Romana Grossová
Faculty of Science, Masaryk University
Department of Theoretical Physics and Astrophysics

Title of Thesis: High Dispersion Spectroscopy with Ondřejov Echelle Spectrograph

Degree Programme: Physics

Field of Study: Theoretical physics and astrophysics

Supervisor: RNDr. Petr Škoda, CSc.

Academic Year: 2015/2016

Number of Pages: viii + 68

Keywords: Echelle spectrograph, IRAF, OPERA, exoplanets

Abstrakt

Ešeletové spektrografy a jejich vysoké rozlišení hrajou důležitou roli při určování charakteristik hvězdných čar. Rosáhle pole aplikací je zaměřeno především na měření přesných radiálních rychlostí. V této diplomové práci se věnujeme kalibraci Ondřejovského ešeletového spektrografu v Astronomickém ústavu Akademie věd České republiky. Mým úkolem bylo vyšetřit široké pole možností, jak zpracovávat data s dosažením nejlepších možných výsledků. Úspěšná redukce byla provedena jak pro Image Reduction and Analysis Facility (IRAF) tak pro Open source Pipeline for ESPaDOnS Reduction and Analysis (OPERA). Tato diplomová práce zahrnuje srovnání obou pipeline.

Abstract

Echelle spectrographs with their high resolution play an important role in the determination of characteristics of stellar lines. A wide field of applications is concentrating mainly on the measurements of precise radial velocity applied in exoplanetary research. In my diploma thesis I am concentrated on the calibration of the Ondřejov echelle spectrograph at the Astronomical Institute of the Czech Academy of Sciences. My role was to investigate the wide field of opportunities how to process the data with the best possible results. Successful reduction was performed by both Image Reduction and Analysis Facility (IRAF) and for Open source Pipeline for ESPaDOnS Reduction and Analysis. This thesis includes the comparison of both pipelines.

Místo tohoto listu vložte kopii oficiálního (podepsaného) zadání práce.

Poděkování

Na tomto místě bych chtěla poděkovat svému vedoucímu Petrovi Škodovi za ochotu, pomoc, vedení a konzultace. Jeho kolegovi Miroslavy Šlechtovi za poskytnutí dat, Zdeňkovi Janákovi za jeho šikovné řešení důležitých problémů, Ederovi Mariolimu za jeho pozitivní přístup, návody, užitečné rady a mailové konzultace, Samuelovi Molnárovi za infromatickou a morální podporu a v neposledné řadě i své rodině a přátelům za podporu.

Prohlášení

Prohlašuji, že jsem svoji diplomovou práci vypracovala samostatně s využitím infromačních zdrojů, které jsou v práci citovány.

Brno 5. ledna 2015

.....
Romana Grossová

Contents

Chapter 1. Introduction	1
Chapter 2. A Brief Introduction to Spectroscopy	2
2.1 The Echelle Gratings	3
2.1.1 The grating equation	4
Chapter 3. The Echelle Spectrographs	10
3.1 Ondřejov Echelle Spectrograph	10
3.2 ESPaDOnS	14
3.3 The comparison of Echelle spectrographs	16
Chapter 4. Exoplanets	19
4.1 Definition and discoveries	19
4.2 Detection Techniques	20
4.2.1 Direct Method	20
4.2.2 Indirect Method	21
Chapter 5. Data files from OES	25
Chapter 6. IRAF	28
6.1 Main Characteristics	28
6.2 Installation	28
6.3 Reduction with IRAF	29
6.4 Final extracted spectra	33
Chapter 7. OPERA	36
7.1 Installation	36
7.2 Wavelength Calibration	37
7.3 Reduction steps	39
Chapter 8. Comparison of spectra from OES	46
8.1 Spectrum of stars in H α	59
Chapter 9. Summary	60
Chapter A. Gnuplot scripts	62

Chapter B. Ruby scripts	64
B.1 Ruby for final data file	64
Chapter C. Manuals	65

Chapter 1

Introduction

As technology goes forward new and more powerful tool appears in each field of science. In case of nowadays astronomy and astrophysics in order to perform our work more effectively and efficiently, we are pushed towards cooperation with the computer science. Therefore, to run more powerful pipeline, the advantage of always improving programming languages need to be included.

Old projects for reduction of astronomical data have been replaced with new ones using more precise programming codes. It is the case of Canada-France-Hawaii Telescope with ESPaDOnS echelle spectrograph. Upena pipeline, which used closed-source Libre-Espirt software, will be soon replaced by OPERA, Open source Pipeline for ESPaDOnS Reduction and Analysis. Disadvantage of closed-source Libre-Espirt is the fact, that it is available only at certain computer machines on Mauna Kea, Hawaii. Whereas, the use of OPERA pipeline can be applied to any other spectrographs in the world.

Fortunately, my supervisor Petr Škoda from the Astronomical Institute in Ondřejov, got in touch with current developer of OPERA and started cooperation in order to apply it to Ondřejov Echelle Spectrograph attached to 2m Perek telescope in Czech Republic, OES. Although Ondřejov already has reduction tool for echelle data called Image Reduction and Analysis Facility, IRAF, it is not working sufficiently. Echelle data from OES has lines tilted with respect to the echelle orders, which is the problem is the problem not solvable for IRAF. That is reason why this thesis is concentrated on producing well functioning pipeline with OPERA software for OES data and analyze the differences between data reduced by IRAF and OPERA. Final comparison of spectra from both tools will be plotted, described and analyzed in order to find the more suitable reduction software for Ondřejov Echelle Spectrograph.

Chapter 2

A Brief Introduction to Spectroscopy

Historically, it has been proved that for getting information about the celestial bodies so far away in the universe, it is useful to investigate incoming electromagnetic waves radiated from them. That is the field of study of spectroscopy. Generally, spectroscopy is a scientific technique, which studies the interaction between electromagnetic radiation and matter. It is a measurement of the radiation intensity as a function of wavelength.

Very famous experiment, made by Isaac Newton in 1666, offered explanation for this theory using the dispersion of sunlight on a prism. He splitted white light to further undistributed colored parts with different index of refraction, that formed a spectrum.

By Thomas Young's inteferometry experiment was explained color assignment to specific wavelength. At the beginning of the 19th century a talented glass maker Joseph von Fraunhofer found several dark lines in a continuous spectrum of the Sun and with the use of telescope he was able to observe spectrum of the Moon, Mars, Venus and several other stars.

The mystery of the dark lines was revealed 30 years later by Gustav Kirchhoff and Robert Bunsen and formed to Kirchhoff's laws of emission and absorption. It is used to determine the composition of celestial bodies from the spectral lines, characteristic for each element. Kirchhoff's law describes equivalent ratio of emissive and absorptive power of rays with the same wavelength at thermal equilibrium.

$$\frac{\epsilon_{\lambda}(T)}{\kappa_{\lambda}(T)} = \text{constant} \quad (2.1)$$

, where the coefficient of emission is ϵ_{λ} , the coefficient of absorption is κ_{λ} , the temperature T and the wavelength is λ . Additionally, the Fraunhofer dark lines and stellar lines can be explained by the Kirchhoff's laws:

- (a) the hot,dense solid objects emit the light with a continuous spectrum
- (b) hot, diffuse gas emits the light only at the specific wavelegths and forms emission spectrum
- (c) and finally, a cool gas absorbing just specific wavelegths of obscured source shows near-continuous spectrum with dark emission lines.

The simplest early spectroscope was a prism. However, the light beam passing through the prism is scattered and absorbed, in any case it can be "lost". Lord Rayleigh demonstrated that diffraction grating represents preferable tool for obtaining higher resolutions. Anyway, several problems raise up in this case, too. The difficulty to produce grating at such quality and the low efficiency as the light disperse into several orders.

Later, the improvement was offered by Fraunhofer. His idea of gratings with many finely ruled apertures on the glass was modified by Lewis Rutherford, who ruled a small number of gratings in metal. At the end of the 19th century the effective manufacturing at John Hopkins University produced "blazed" gratings with ability of light diffraction up to 50 % into first order.

After the interchangeable prisms and gratings in spectrograph of Lick refractor, the Cassegrain spectrograph was constructed. It enhanced several advanced techniques for flexed control and was used at the Cassegrain focus of the telescope. The light coming into the telescope was reflected by primary and secondary mirror to the Cassegrain focus and spectrograph. Then it passed through the slit and the parabolic mirror collimated it to the diffraction grating. The spectrum was formed and focused by lenses onto the photographic plates(nowadays, it is mostly used a charged couple device, CCD).

Furthermore, flexure problems were eliminated by construction of a coudé spectrograph located at the coudé focus. The light was reflected by mirrors to the telescope axis, where the coudé slit room was located. Then the light beam passed through the slit of the spectrograph to the diffraction element forming spectrum onto the photographic plate.

First, the prisms were used as a diffraction element, later were replaced by blazed gratings and finally by Schmidt camera. In order to gain the highest resolution, the large gratings¹ and the large photographic plates with the long focal length cameras were installed. Ideas of this methods were firstly used at the Mt Wilson spectrograph and after that it was spread to many observatories around the world and used ever since.

2.1 The Echelle Gratings

Generally, the most important factor of a diffraction gratings is resolution. It is proportional to the total number of grating rules N and the order of diffraction m . When the highest resolution wants to be achieved, the main goal should be followed:

- increasing the number of grating rules
- increasing the order of diffraction.

Subsequently, the larger and more finely ruled grating had been used. As it was mentioned in previous section, the most effective setup was with the coudé spectrograph.

However, blazed gratings achieve to disperse the light only into second and third order. Albert Michelson's experiments of an "échelon" consisted of a small number of parallel plates made of glass. The resolving power of the order of one million was achieved in 1933 by Williams. At that time conventional grating "échelette" ruled on metal was designed by R.W.Wood.

¹With no limit for the space of the Cassegrain focus.

And finally, nowadays well known and all around the world used "echelle" grating was described by Harrison in 1949. The word "échelle", in french, means stairs or ladder. There are several differences between conventional and echelle grating. Mainly, echelle represents an compact and high-resolution instrument. This statement is result of few properties it holds. Echelle has less grooves per millimeter than échellette and is used at high angles into high diffraction orders, so that it is more efficient and has low polarization effects over the large spectral intervals.

The product of such high-resolution grating represents overlapping orders separated by crossed low dispersion element. Usually, prism, grism or exceptionally another grating is used as a cross-disperser.

2.1.1 The grating equation

This subsection is offering important echelle grating equations. Firstly, it is concentrated on a standard diffraction grating. Fig. 2.1 is showing its schema in both pictures. Picture **b)** showing the standard grating with an incident angle γ with respect to the facet normal.

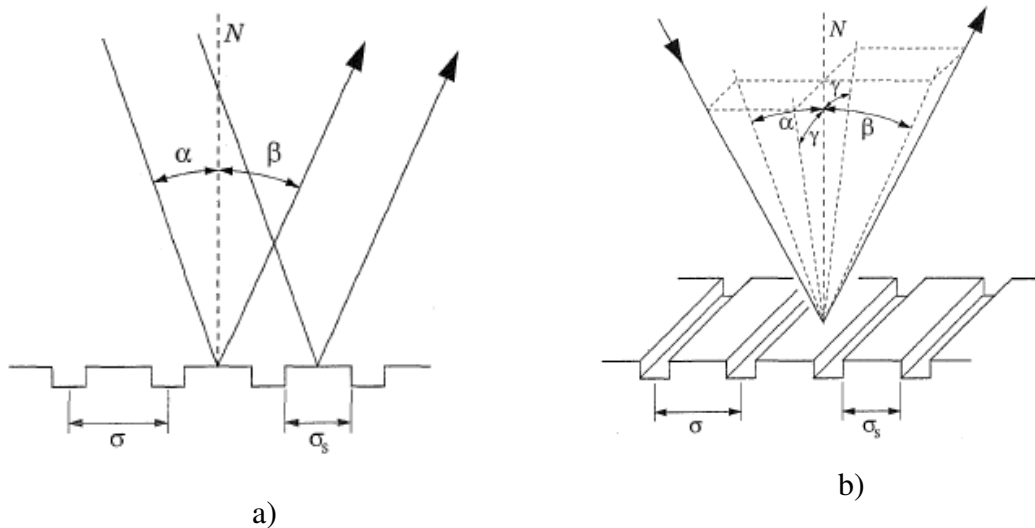


Figure 2.1: Schematic diagrams of a standard diffraction grating: **a)** all beams parallel to grooves and **b)** incident angle γ with respect to N . [1]

Grating is composed of reflective "tooth" or grooves with a normal N and parallel rules with a spacing σ . The light incidents at the angle α and reflects at the angle β . Total path difference between grooves forms a standard grating equation:

$$m\lambda = \sigma (\sin\alpha \pm \sin\beta) \quad (2.2)$$

and for the inclination angle γ additional term will appear:

$$m\lambda = \sigma (\sin\alpha \pm \sin\beta) \cos\gamma. \quad (2.3)$$

This condition posses the plus sign, if the diffracted beam is on the same side of the grating as the incident beam. Otherwise, it is negative.

Huygen's principle stands that each groove facet with width of σ_s is a source of secondary spherical wavelets.

Constructive interference will occur, if diffracted beam path differs by an integer wavelength number ($m = \pm 1, \pm 2, \dots$). It will interfere destructively if m is $\pm 1/2, \pm 3/2, \dots$

As the most of the light is reflected into a zeroth order, wavelengths start to overlap. The solution is offered by blazed reflection gratings. The position of the grating can be tilted so, that the incident (α) and diffracted ($\bar{\beta}$) beam are at almost the same angle, in order to direct them towards preferable direction. For instance, towards the specific diffraction order.

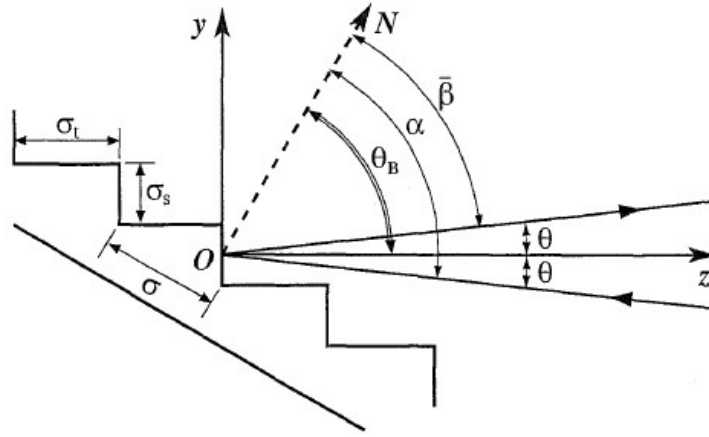


Figure 2.2: Profile image of grating and blaze angle θ_B . [1]

Profile of the tilted grating is shown in Fig. 2.2. The two angles, incident α and diffracted $\bar{\beta}$, are measured from grating normal and third angle θ_B is measured from facet normal to the light beam. Next relations can be applied:

$$\alpha = \theta_B + \theta$$

$$\bar{\beta} = \theta_B - \theta \quad (2.4)$$

$$\Rightarrow \alpha + \bar{\beta} = 2 \theta_B. \quad (2.5)$$

Taking under account very polished surfaces, the peak intensity in diffraction matches the specular reflection of the groove facet, α and $\bar{\beta}$ are equal. Only single outgoing angle is produced and it's called blaze angle θ_B .

Moreover, the blaze wavelength λ_B can be defined as :

$$\begin{aligned} m\lambda_B &= \sigma (\sin\alpha \pm \sin\bar{\beta}) \cos\gamma \\ &= \sigma \sin\theta_B \cos\theta \cos\gamma \end{aligned} \quad (2.6)$$

Efficiency of grating operation is limited to only viable modes, where $\alpha > \bar{\beta}$ or $\alpha \approx \bar{\beta}$. Let's consider the Littrow condition, when $\alpha = \bar{\beta}$ that means $\theta = 0$ and quasi-Littrow, when $\gamma \neq 0$. Considering this condition, the optical depth of a grating σ_t is:

$$\sigma_t = \sigma \sin\theta_B \quad (2.7)$$

and facet width is given by:

$$\sigma_s = \sigma \cos \theta_B \quad (2.8)$$

That was last step of determining the order of interference for diffracted light:

$$m = \frac{2\sigma_t}{\lambda} \quad (2.9)$$

Grating with large blaze angle are nothing less than echelle grating. The name "R-number" is given by the tangent of the blaze angle. For instance, R2 grating with an angle $\theta_B = 63.4^\circ$.

Cross-disperser

As mentioned before, echelle grating produces overlapping orders ($m \gg 1$), which is separated by the second dispersive element, prism, grims or grating (Fig. 2.3). The two Figs. (2.4 and 2.5) underneath give a comparison between orders imagined by prism and grating. Grism represents the combination of prism and grating in order to get light at chosen wavelength passed straight through.

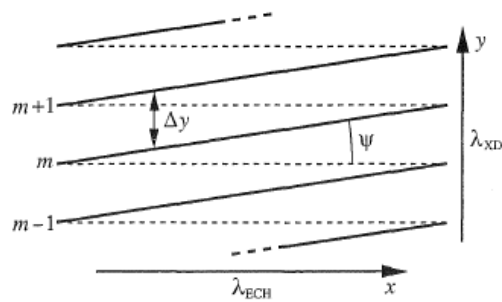


Figure 2.3: The schema of cross-dispersion and cross-disperser grism.[1]

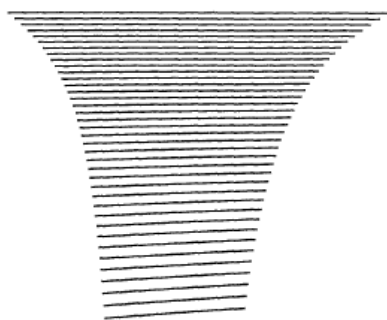


Figure 2.4: a)

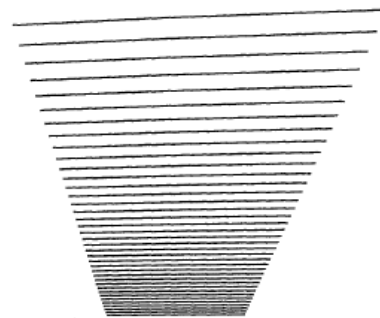


Figure 2.5: b)

Orders with: a) prism and b) grating.[1]

The order separation

Additionally, the condition of the separation between orders can be applied:

$$\Delta y = f_{\text{cam}} \frac{d\beta}{d\lambda_{\text{XD}} \Delta\lambda_{\text{FSR}}}, \quad (2.10)$$

where f_{cam} is the focal length of spectrograph camera, $\frac{d\beta}{d\lambda_{\text{XD}}}$ is the angular dispersion of the cross-disperser and $\Delta\lambda_{\text{FSR}}$ is the free spectral range.

The free spectral range is an changing wavelength from an order m to the next ($m \pm 1$):

$$\Delta\lambda_{\text{FSR}} = \frac{\lambda}{m}, \quad (2.11)$$

Each wavelength in order m is also present in orders ($m \pm 1$).
noindent

Let's consider blaze wavelength λ_{B} in equation for free spectral range:

$$\Delta\lambda_{\text{FSR}} = \frac{\lambda_{\text{B}}^2}{2\sigma \sin\theta_{\text{B}} \cos\theta \cos\gamma}, \quad (2.12)$$

and apply it to the order of separation:

$$\Delta y = f_{\text{cam}} \frac{d\beta}{d\lambda_{\text{XD}}} \frac{\lambda_{\text{B}}^2}{2\sigma \sin\theta_{\text{B}} \cos\theta \cos\gamma} \quad (2.13)$$

The resolving power

The resolving power is very important property of any spectrograph. The smallest wavelength difference $\Delta\lambda$ between two spectral lines, that are able to be distinguished at wavelength λ , defined as:

$$R = \frac{\lambda}{\Delta\lambda}, \quad (2.14)$$

where $\lambda \approx \lambda_1 \approx \lambda_2$.

Angular dispersion

The angular dispersion applied into the relation, will give:

$$R = \frac{\lambda}{\delta\beta} \frac{d\beta}{d\lambda}, \quad (2.15)$$

where $\delta\beta$ is an angular width between two wavelength in the dispersed beam, followed by angular dispersion $\left(\frac{d\beta}{d\lambda}\right)$.

Importantly, the effect of anamorphic magnification (Fig. 2.6) needs to be considered. The source, viewed from grating at angular distance $\delta\alpha$, has after dispersion angular separation $\delta\beta$:

$$\delta\beta = \delta\alpha \frac{d\beta}{d\alpha} \quad (2.16)$$

An anamorphic magnification is described in following equation:

$$r = \left| \frac{d\beta}{d\alpha} \right| = \frac{\cos\alpha}{\cos\beta} \quad (2.17)$$

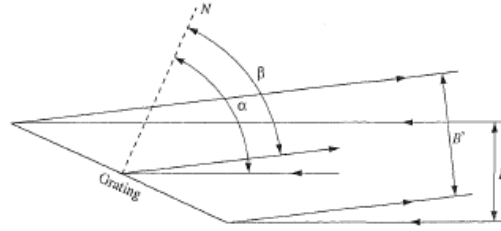


Figure 2.6: Anamorphic magnification on dispersed light from echelle grating.[1]

Furthermore, amortification can be applied to the relation of resolving power and it becomes:

$$R = \frac{\lambda}{\delta\alpha} \frac{d\alpha}{d\lambda} \quad (2.18)$$

Or, when the relation $\frac{d\alpha}{d\lambda} = \frac{\sin\alpha + \sin\beta}{\lambda \cos\alpha}$ is applied:

$$R = \frac{1}{\delta\alpha} \frac{\sin\alpha + \sin\beta}{\lambda \cos\alpha} \quad (2.19)$$

$$= \frac{1}{\delta\alpha} \frac{2 \tan\theta_B}{1 - \tan\theta_B \tan\theta} \quad (2.20)$$

In addition, the diffraction limitation on resolving power needs to be include too. Grating of length L , with the number of grooves N across it, gives the limit:

$$m\lambda = \frac{L}{N} (\sin\alpha + \sin\beta) \quad \text{and} \quad (2.21)$$

$$R = mN. \quad (2.22)$$

In diffraction limit, when the collimated beam size is B equal to $(L \cos\alpha)$ and the limit of angular size of a slit is $\approx \lambda/B$.

Linear Dispersion

Linear dispersion determines the range of wavelengths, that will fit onto the detector at the focal plane of the spectrograph. Let's consider α to be the same for all wavelengths.

Consequentially, for the given m the differentiation of the grating equation 2.2 will give:

$$m = a \cos\beta \frac{d\beta}{d\lambda} \Rightarrow \frac{d\beta}{d\lambda} = \frac{m}{a \cos\beta}, \quad (2.23)$$

where a is the number of lines per mm. Then the spectrum is linearly dispersed at x-direction in camera's focal plane f_{cam}

$$\frac{dx}{d\lambda} = f_{\text{cam}} \frac{d\beta}{d\lambda} = \frac{m f_{\text{cam}}}{a \cos\beta} \quad (2.24)$$

The resolving power can be derived from reciprocal form of the linear dispersion in Å/mm and with well known size of a pixel on CCD. It will give the dispersion per pixel, the smallest distinguishable wavelength $\Delta\lambda$ (in Å) in equation for resolving power (2.14).

Two previous sections were made from [1] and [2].

Chapter 3

The Echelle Spectrographs

The aim of this chapter is to introduce and compare echelle spectrographs all around the world. The closer look is taken at the Ondřejov Echelle Spectrograph (OES) at 2m telescope in Ondřejov, Heidelberg Extended Range Optical Spectrograph and the Echelle SpectroPolarimetric Device for the Observation of Stars at Canada-France-Hawaii Telescope on Hawaii. The first spectrograph, as the main topic of this thesis. The second one, as an inspiration for constructing OES and the last as the main reason why the new project for reduction and analysis was produced.

3.1 Ondřejov Echelle Spectrograph

In 2000, the research team under the lead of P. Koubsky of stellar astronomy at Astronomical Institute of the Czech Academy of Sciences in Ondřejov decided to construct an echelle spectrograph (OES). The spectral region limitation was the main reason why a standard coude spectrograph was not sufficient enough. As an inspiration served echelle spectrograph HEROS (Heidelberg Extended Range Optical Spectrograph) from Germany.

HEROS is a fiber fed spectrograph designed and build by Andreas Kaufer, et al. in 1994. The light from the telescope is carried by 10m fiber, which has an 100 micron core diameter. Since the end of fiber represented the point source, slit is not required. Echelle grating has 31.6 grooves/mm with an blaze angle 63.4 deg (R2 grating) and contains two separate camera channels with different wavelength ranges, red (365-565nm) and blue (580-835nm). That means HEROS is possible to cover at once around 400nm-long part of a spectrum, almost 10 times more than can cover standard spectrograph in Ondřejov, with circa twice bigger resolving power.

In testing process, HEROS was attached to the Cassegrain focus and more than 1500 spectra were obtained, although, some problems had arisen. Mainly, by merging the orders reflected to variability of wave-like structures of continuum. The problem remained after flat-fielding and was not overcome.

After 4 years of gathering experiences was Ondřejov echelle spectrograph fully functional. Although, HEROS was great inspiration some changes in construction of OES needed to be done.

OES is a slit spectrograph. For the fiber-fed mode the fiber would need to be 20m long, as the light travels from primary or Cassegrain focus.

In fully operational mode, OES is stored in the room build symmetrically to the coudé focus of 2m telescope and to the room for standard spectrograph¹ as it is illustrated in Fig.3.1. Since in the coudé focus is situated a plane mirror, it is possible to switch between two spectrographs within a night.

Additionally in this setup fiber would represent only redundant optical element.

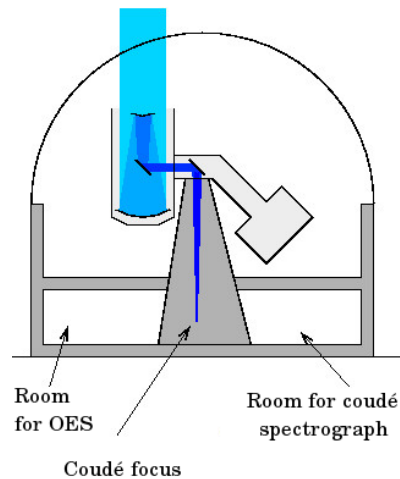


Figure 3.1: Location of Ondřejov Echelle Spectrograph.[20]

Schema of OES

The schema of the setup of important optical parts of spectrograph and the light beam passing through shows Fig.3.2. Additional information will be considered.

Left hand side part of Fig. 3.2 shows setup for OES. The light beam, painted in red, is coming from the coudé focus through a 0.6mm slit (A), at distance 500mm from the front edge of the grating (C). Next, the beam is converted to a parallel beam by the collimator No.1 with the focal length $\approx 4600\text{mm}$. The optical diameter of the collimator and as well the diameter of produced beam is approximately 150mm. The most important optical part, echelle grating (C), was constructed by Milton Roy, has a blaze angle of 69° ($\tan \approx 2.6$), 54.5 grooves/mm and the size $154 \times 408\text{mm}$. Produced spectrum, with overlapping orders, is pictured on a parabolic mirror (D) with focal length approximately 1100mm and it is reflected on small mirror (E) with an 45° angle of inclination and next to the second collimator (F), with almost 600 mm smaller than the focal length of parabolic mirror (D). Last optical element represents cross-disperser (G), prism from a glass Schott LF5² with an vertex angle 54.5° . Spectral orders, divided by prism, are filling up the $30 \times 10.5\text{mm}$ area in focus of 200mm camera (H)-Canon EF. The beam incidents at the angle 46.8° . The mean deviation at 480nm is 38.6° . [8]

¹The difference is that standard spectrograph has only one disperse unit (prism or grating)

²LF means "light flint"

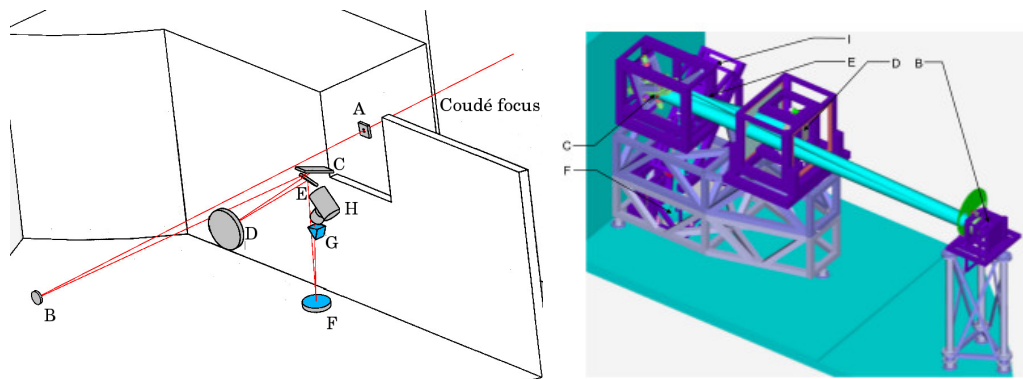


Figure 3.2: Schematic setup of OES: A)Slit, B)Collimator No.1, C)Echelle grating , D)Parabolic mirror, E)Additional flat mirror, F)Collimator No.2, G)Prism, H)Lens of camera. I)CCD detector (right picture).

[8]

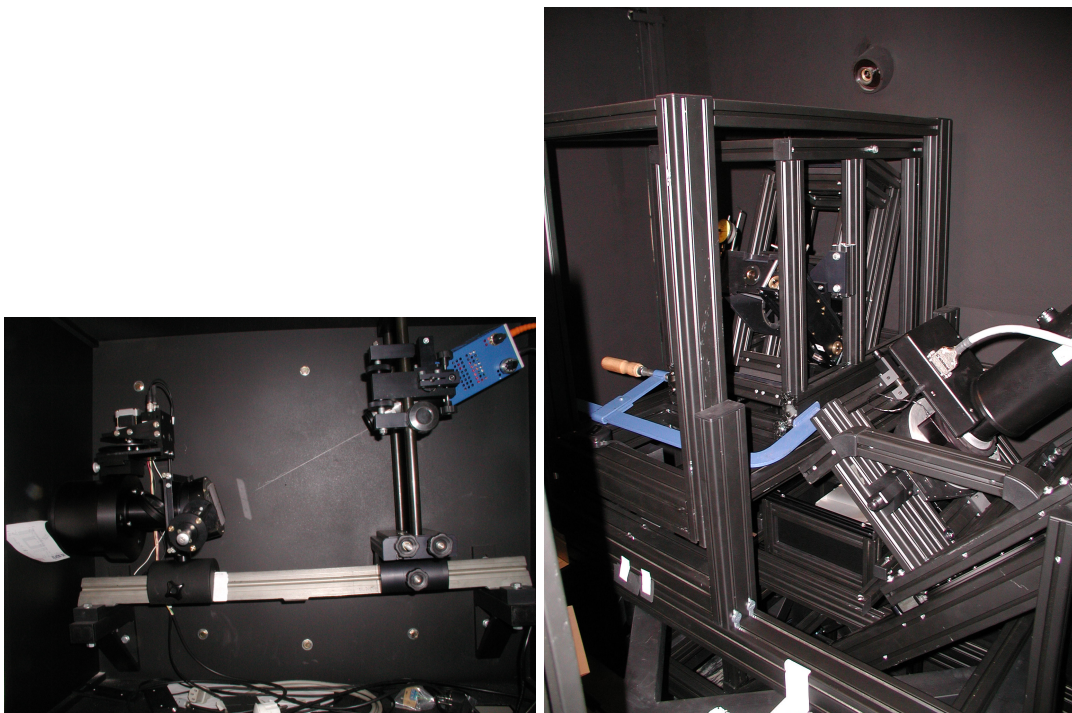


Figure 3.3: Ondřejov Echelle Spectrograph. Pictures were obtained from server of Stellar Department.

Iodine Cell

For high-precision spectroscopy can OES use the iodine cell as well.

The Iodine (I_2) absorption cell is a vacuum sealed glass jar with Iodine crystals and is wrapped with heat ribbon to warm it on working temperature. Iodine sublimes at this temperature 35° , while the working temperature is typically at $60-80^\circ$, and produces a spectrum of an deep and very narrow absorption lines in range of waveleght between 4800 \AA and 6100 \AA , whereas the highest absorption is in range from 5100 \AA till 5600 \AA as

demonstrates Fig. 3.4. This generated spectrum represents very stable zero-velocity reference system.

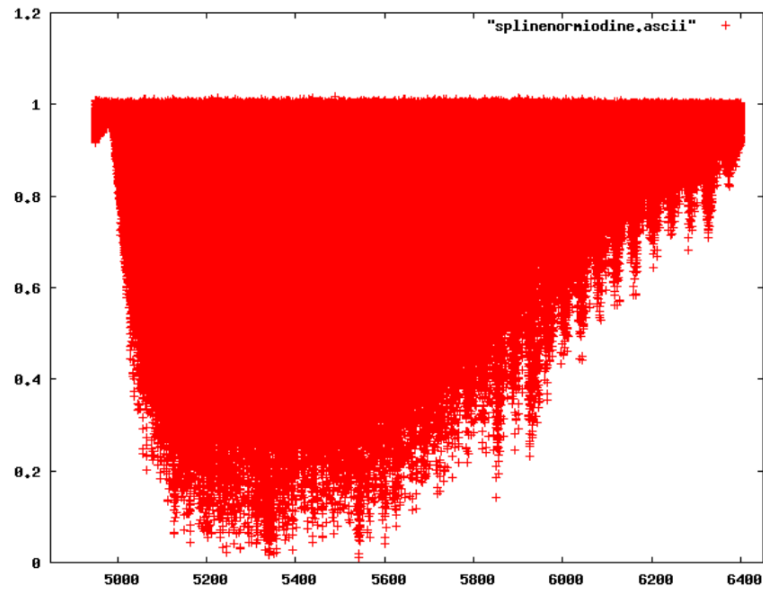


Figure 3.4: Iodine cell spectral range.

Although, some observations with iodine cell in Ondřejov have been already performed, further research and adjustments are required in this field. Sample data with Iodine cell are presented in last section, which includes final extracted spectra from both OPERA and IRAF.

Spectral range

The Ondřejov echelle covers visible spectral range from 3870 Å to 10100 Å³ in 42 orders recorded on 2048×2048 EEV chip in an Dewar jar. The distance between orders is 12 pixels in red part of a spectrum and 27 pixels in blue. Additionally, one pixel has size 13.5 μm.

Spectral resolving power

Determination of resolving power is complex problem. It can be precisely determined only by measured by laser. However, for approximate estimation is sufficient enough to just calculate practical value from two pixel resolution or theoretical value from parameters of instrument, particularly grating and detector.

In practice, it is possible for OES to get spectral resolving power for each line separately. An example reduction of V1679 Cygni by M. Šlechta shows, that the wavelength 5000Å belongs to 21st order. The value of CDELTA1 = 0.0407419 is found in the header

³Although in infra-red part is influenced by very bad fringing and Thorium-Argon calibrations. In this part are missing or are not applicable.

of V1679 Cyg. Center is around 5010 Å , where the value 0.041 Å is the distance between centers of two neighbouring pixels and those two pixels are 0.082 Å apart. Spectral resolving power for two pixels is:

$$R = \frac{\lambda}{\Delta\lambda} = \frac{5010}{0.082} = 61100 \quad (3.1)$$

Considering H α line, the order 38 is investigated. Center of this order is located around 6590 Å with the distance between two pixels 0.05362. What gives the resolving power for H α :

$$R = \frac{\lambda}{\Delta\lambda} = \frac{6590}{0.011} = 61450 \quad (3.2)$$

Theoretical resolving power was derived by Pavel Koubsky in the article [8]. Considering estimated linear dispersion from observation (values of CRVAL in header) on the value 2,4 Å/mm at 5000Å, the width of the slit is 600 μm , than image would have 40 μm (almost more than three 13.5 μm pixels) in the camera, what leads to the resolution 51 600 at 5000 Å. Two pixel resolution is 77000. Important is to note, that those are just approximate values. After extraction of stars by OPERA, its statistics showed the value not higher than 56000.

Now we focus on the spectrograph, which was the inspiration for the production of the new reduction tool.

3.2 ESPaDOnS

ESPaDOnS is an **E**chelle **S**pectro**P**olarimetric **D**evice for the **O**bservation of **S**tars at 3.6m Canada-France-Hawaii Telescope. Design and the construction was made by a team of 15 scientists, engineers, technicians, and administrators at he Observatoire Midi-Pyrénées in France inspired by FEROS spectrograph.

Two units forms ESPaDOnS, bench-mounted fiber-fed echelle spectrograph and on telescope attached Cassegrain unit, which includes polarimeter, calibration unit and camera, all connected with 30m of fiber. Spectroscopic analysis is concerned with tree modes: standard spectroscopy, spectropolarimetry and for the very faint objects standard spectroscopy with subtracted spectrum of the sky. Beside the uniqueness in measuring the magnetic topogies of stars, ESPaDOnS is used for galactic objects, stellar and planetary studies.

Spectrograph is stored in thermal enclosure on third floor of Coudé room. This way the affects on spectrograph by temperature and pressure fluctuation are minimized.

Interesting fact is, that with the longest 270m fiber ever made is ESPaDOnS connected to its 8m neighbour telescope. This project is called GRACES, Gemini Remote Access to CFHT ESPaDOnS Spectrograph, and works in the same modes, except polarimetry. Access is granted when spectrograph is not used by the CFHT. In 2016 the bilateral agreement will be executed. The CFHT community will be able to use theirs telescopes, Gemini North or South, with ratio 3/20 nights.[11]

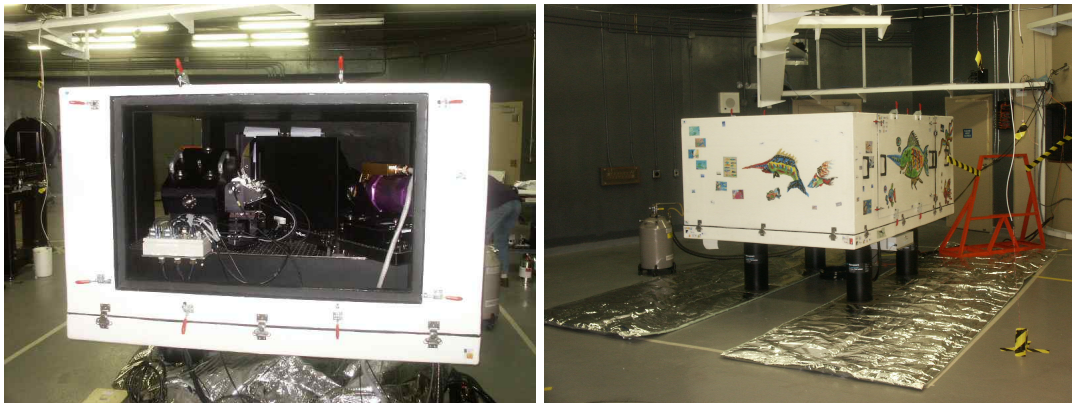


Figure 3.5: ESPaDOnS in its thermal enclosure, in the 3rd floor Inner Coudé room.[25]

Schema of ESPaDOnS

This echelle spectrograph is working in dual pupil and quasi Littrow configuration. Setup of optical parts is shown on Fig. 3.6.

The light is fed by optical fibers to the Bowen–Walraven image slicer made of three individual prisms for transforming the circular images into the narrow strip at the spectrograph slit level. The statics claim, that about 40 % to 45 % of stellar photons made it from the telescope to the spectrograph. After slicing, the light is collimated by the main collimator to the diffraction grating and back to it, forming the first overlapping spectrum near to the flat mirror. It's role is to send the beam to the transfer collimator and to the cross-disperser, in this case the prism. Thereafter the final image is recorded onto 2048x4096 15 micron pixel CCD detector of the fully dioptic camera with 388mm focal lens and with free diameter of 210mm.

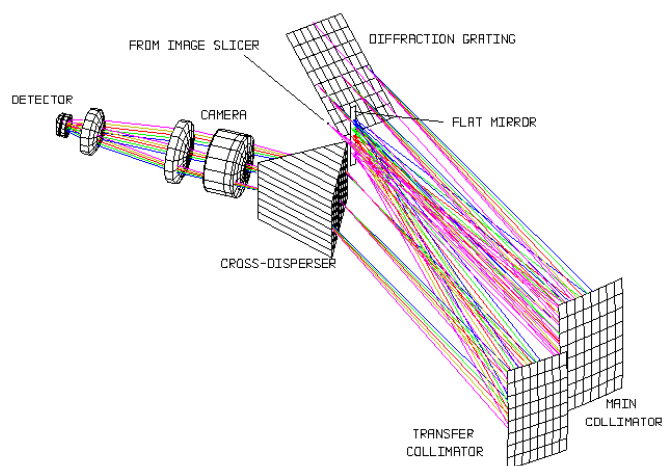


Figure 3.6: The schema of spectrograph.[26]

Spectral range and resolution

ESPaDOnS covers not only the visible part of the spectrum from 370nm to 740nm, but also continues to near infrared part till 1050nm⁴ in a single exposure. It provides spectral coverage of 40 orders from the order 61 to the order 22. Echelle R2 grating has 79 grooves per mm, the size 200x400mm.

Spectral resolution differs depending on mode that is used. Considering sky and standard spectroscopy and spectropolarimetry the resolution reaches 68 000, whereas for standard spectroscopy only the resolution increases, up to 81 000.

3.3 The comparison of Echelle spectrographs

The short overview of the echelle spectrographs is presented in the Table 3.1. It includes samples from all around the world. Two German spectrographs from Heidelberg and Tautenburg, SOPHIE in Haute-Provence Observatory in France, Netherlands UES on one of the Canary Island, La Palma, attached to the William Herschel Telescope and Belgium HERMES at the Mercator Telescope and at last ESO facility HARPS at 3.6m and FEROS at 2.2m telescope in La Silla, Chile.

HERMES and SOPHIE have two modes available with different spectral resolving powers. Firstly, HERMES has high resolution mode (HRF) with $R \sim 85\,000$ for high efficiency along with simultaneous wavelength reference mode (LRF) with R up to 62 000 for high instrument stability. In the case of SOPHIE, high resolution mode (HR) with $R \sim 75\,000$ achieved by 40 μ m slit and HE as high efficiency mode concentrating on fainter objects with 25 000 smaller spectral resolution.

Cross-dispersing element is indispensable for each echelle spectrum. Table 3.1 shows, that in most cases this role represents prism. Remaining spectrographs are using grism, so called grating prism.

ESO's HARPS holds first place for the highest resolving power. On the other hand, German HEROS takes the last place. Whereas the longest spectral range is covered by UES. Certainly, the range is not completely continuous, small gaps in between two parts of the spectrum are included.

As a matter of fact, HARPS takes the highest places especially in field of low-mass exoplanetary research, as its name implies. Statistics from 2010 stands, that HARPS discovered 23 of 28 exoplanets with mass 18 times smaller than Earth mass. The rate is still increasing. Unquestionably, because of sub-ms⁻¹ precision of radial velocity determination. On the other hand, new-generation spectrograph ESPRESSO is optimized for discoveries of non-active rocky planets of few Earth masses.

⁴Three small gaps in infrared are included.

Table 3.1: The comparison of echelle spectrographs. [14],[13],[9],[17],[20],[25],[27].

Short cut	Name	Resolving power	Spectral range[Å]	Cross-disperser	Fibre-fed
OES	Ondřejov Echelle S.	50000	3870-10100	prism	no
ESPaDOnS	Echelle SpectroPolarimetric Device for the Observation of Stars	81000	3700-10500	prism	yes
HEROS	Heidelberg Extended Range Optical S.	20000	3450-8650	prism	yes
FEROS	The Fiber-fed Extended Range Optical S.	48000	3500-9200	prism	yes
HARPS	High Accuracy RV Planet Searcher	115000	3780-6910	grism grism	yes yes
ESPRESSO	Echelle S. for Rocky Exoplanets and Stable Spectroscopic Observations	HR:134000 MR:59000 UHR:200000	3800-7800	prism	yes
UES	Utrech Echelle S.	54000	3000-11000	prism	no
	Echelle Tautenburg	67000	3400-9270	grism	no
HERMES	High Efficiency and Resolution Mercator Echelle S.	HRF:85000 LRF:62000	3770-9000	prism	yes
SOPHIE	Spectrograph for Observation of Phenomena of stellar interiors and Exoplanet	HE:75000 HR:40000	3870-6940	prism	yes

The data gathered in the Table (3.1) suggests that optical fiber for transmitting the light from the telescope to the spectrograph are frequent component of those instruments.

Since 1970 the optical fiber are often used in spectroscopy. Optical fibers (3.7) are made of glass or plastic with higher reflective index than cladding, which is covering the fiber. Once the light is reflected at larger angle than the critical angle, is totally internally reflected. This principal is essential for functioning of fibers. The buffer is for mechanical protection.

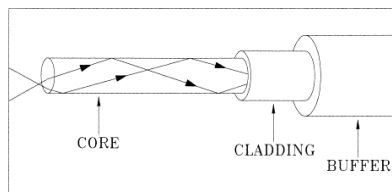


Figure 3.7: The construction of optical fiber. [12]

To main advantages of this instrument belongs high flexibility, more mechanically stable spectra, multi-fibers observation spectroscopy, integral field spectroscopy and slightly higher spectral resolution than slit, because of circular apertures. On the other hand, some

problems by using fiber have arisen. Internal transmission, absorption and circular aperture losses, focal-ratio degradation⁵, variance of light flux along the observation, constant core diameter not adjustable to seeing condition. For telescope with different than coudé or Nasmyth feed, are optical fibers very convenient.

One of the most important capabilities of echelle spectrograph, high resolution, offers possibility to explore important fields of stellar physics unreachable for standard spectroscopes.

Gradually, larger and larger telescopes are constructed, what extends the capability of spectrograph to reach to the fainter objects. As the photon collective power increases too, the high precision spectroscopy is in demand. With precise spectroscopy the instrumental effects on spectra can be reduced, what results in providing highly repeatable observations over long timescales. Most importantly, the determination of the position and shapes of spectral lines are included, mainly the high precision measurements of radial velocity. ESO-ESA⁶ working group's report from 2005 states, that those velocity instrumentation are for further following-up of the astrometric and transit detection methods of exoplanets, to ensure detection by this second method and determining its true mass. Along the support experiments are provide to improve radial velocity mass detection limits.

The search for terrestrial planets in habitable zones is considered to be one of the leading topics of the next decades in Astronomy. Moreover, it represents important application of the purpose of high dispersion spectrographs. That is the reason why next chapter of this thesis will be dedicated to the topic of exoplanets.

⁵The emergent light has lower focal-ratio than input light is more spread out in an angle.

⁶ESO stands for European Organization for Astronomical Research in the Southern Hemisphere and ESA for European Space Agency

Chapter 4

Exoplanets

4.1 Definition and discoveries

Exoplanet (extra solar planet) is known as a planet, that orbits other star than Sun.

That brings out a question, how is actually the word "planet" defined? As it was agreed in February 2003 by the Working Group on Extrasolar Planets (WGESP) of the International Astronomical Union, "planet" by its definition is an object with true masses below the limiting mass for thermonuclear fusion of deuterium.¹ On the other hand the substellar objects above this limit are define as "brown dwarfs", not considering their location of the origin or the process of the formation.

Existence of exoplanets was predicted in 18th century by Immanuel Kant. In those times it was just an idea, because there was no possible way how to prove it. First exoplanet was discovered by Alex Wolszczan and Dale Frail in 1992 unexpectedly around a pulsar. Three years later Michel Mayor and Didier Queloz of the University of Geneva found an exoplanet around the star 51 Pegasi b², main-sequence star, that has triggered the boom of the exoplanets discoveries.

Fig. (4.1) below shows the numbers of discoveries from 1992 till nowadays with both direct and indirect methods, that can be used to find new extrasolar planets. As of the October 2015, about 1968 planets had been discovered in 1248 planetary systems, including 490 multiple systems. This data is available on The Extrasolar Planets Encyclopedia in their catalog. The biggest increase was observed around year 2014, mainly because of discoveries made by Kepler spacecraft. It will be described in the section about the transit detection.

¹Calculated for objects of solar metallicity to be $\sim 13 M_J$ (Jupiter masses)

²The naming convention for exoplanets stands of the star's name, which the exoplanet wandering about, followed by "b","c"...in the order of the planet's discovery.

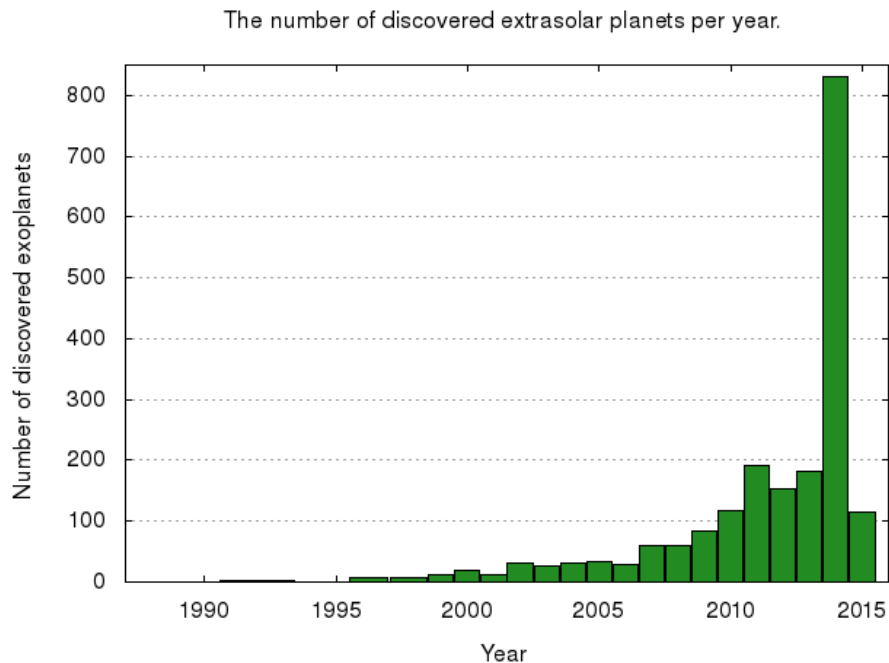


Figure 4.1: The number of discoveries per year for all methods.

4.2 Detection Techniques

Exoplanets are really difficult to detect and imagine, as a result of a small angular separation and a large brightness contrast between the planet and the star. The problem with contrast can be partly solved by looking at the dimmer stars such as white and brown dwarfs. Although, there are no discoveries whatsoever around white dwarfs, but there were found several planets around brown dwarfs by the Very Large Telescope.

4.2.1 Direct Method

Usually, all of the exoplanets discovered by direct method are widely separated from the star and also have bigger mass than Jupiter. The majority of these planets have high temperatures, because they radiate in infrared wavelength so they are fainter in visible light. In some cases³ it is preferable to make observation at 656,281 nm, well known wavelength for hydrogen line, $H\alpha$, because planets are more luminous at this wavelength than in near-infrared. That is the reason, why more $H\alpha$ surveys are undertaken [3].

Currently, several surveys exist for direct-imaging detection of exoplanets, namely Gemini Planet Imager, VLT-SPHERE and SCExAO.

On the other hand, there is a possibility to detect the planet near the planet's Planck peak, what opens up the problem, that none of an achievable telescope would be sufficient enough for longer wavelengths, because of the diffraction limit of an angular resolution.

³The formation of young giant planets during accretion phase.

4.2.2 Indirect Method

More successful approach is indirect detection methods. It takes advantage of the influence of the planet on dynamics or brightness of the host star. The most effective methods are:

- the radial velocity or Doppler method
- the astrometry
- the planetary transits
- the transit–timing variation (ttv)
- the timing
- the microlensing

Fig. (4.2), constructed by the data from [21], shows the comparison between exoplanetary discoveries by all known methods, in both direct and indirect way. The highest peak contains data from 2014 gained by transit method, as mentioned before, therefore additional graph is embedded with only astrometry, timing, imaging, microlensing and ttv.

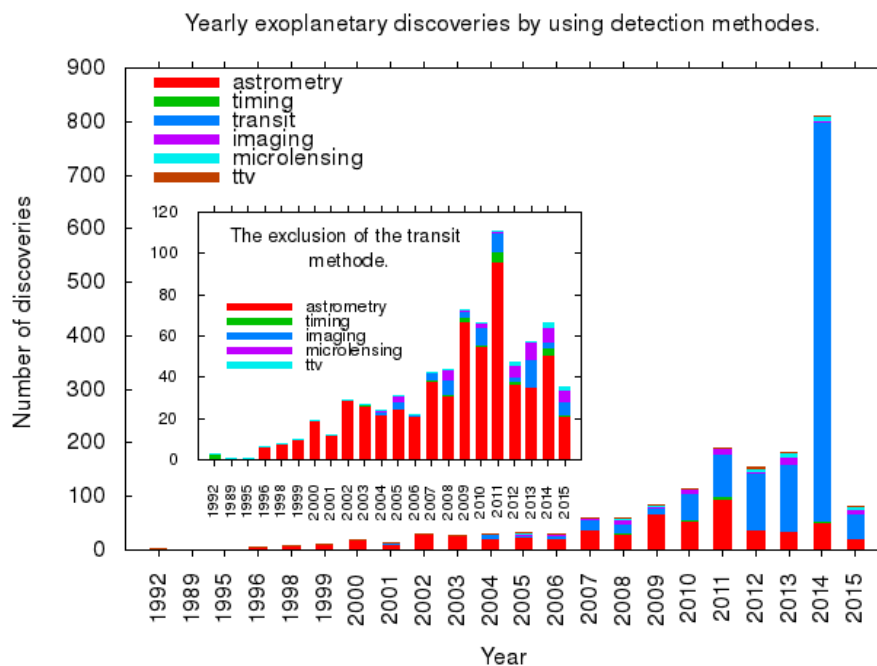


Figure 4.2: Exoplanetary discoveries per year for different detection methods. Data from [21].

The Radial Velocity Detection

The RV method is mostly covered by high-precision measurement from echelle spectrograph, as mentioned before. It uses the detection of the radial velocity v of the star with mass M_* as the planet with mass M_p rotates around their centre-of-mass a at the distance $2a M_p / (M_p + M_*)$ from the star. Let's assume that $M_* \gg M_p$ and the angle between the normal of the plane of planet's orbit and the flow line between the star and the observer is the inclination i , then the condition for the velocity of the star stands the equation:

$$v^2 = G \frac{(M_p \sin i)^2}{2M_* a} \quad (4.1)$$

The useful results of this method is that it is able to determine $(M_p \sin i)$ and planet's orbit eccentricity e from the shape of time variation of velocity.

On the other hand, important disadvantages rises up with unknown inclination angle of the orbit, so it is possible to determine only the lower limit on the planet's mass.

It is mostly used for G and K type, low mass stars, closely orbited by larger mass planets, in order to get the largest vision field of stellar velocity and it should offer the best possibility how to distinguished between the natural turbulent velocity in a photosphere and studied radial velocity due to planetary orbit.

Astrometry

Astrometry is measuring the time changes of the position of the star in the sky. Planet's gravitational influence, causing reflex motion of the star, can be recognized. It is especially useful for describing and completing properties known from the other detection methods, for instance the absolute mass and orbital inclination of the planet.

Let's consider the star and the planet moving around the same center-of-mass, than the reflex amplitude of the star gives:

$$a_* = a_p \frac{M_p}{M_*}, \quad (4.2)$$

where a_* is the distance of the star from the centre-of-mass a the same for the planet (a_p).

This method is the most suitable for the systems near from the Earth, because it measures an actual angular position of parent star.

The European Space Agency mission Gaia, launched at the end of 2013, contributes as well to astrometric detection. It's microarcsecond-precision of stellar positions will help to investigate the properties gained by another methods. It aims to detect over ten thousand Hot Jupiters⁴ and will affirm the existence of Jupiter-size planets from Doppler method [4].

⁴Hot Jupiters(or epistellar Jovians) are one type of exoplanets with Jupiter's characteristics. However, the very close orbit around the host star, causes much higher surface temperatures than for Jupiter. Bellerophon, or 51 Pegasi, is well known representative of this class.

Transit Detection

Gaia is used for transit detection only in conjunction with ground-based observation. Otherwise, it would rather give results for adventitious timing of the transit, because the time sampling of Gaia is weakly distributed [4].

Transit method consists of measuring the decrease of the intensity of parent star as planet transits in front of its disk as seen in Fig. 4.3.

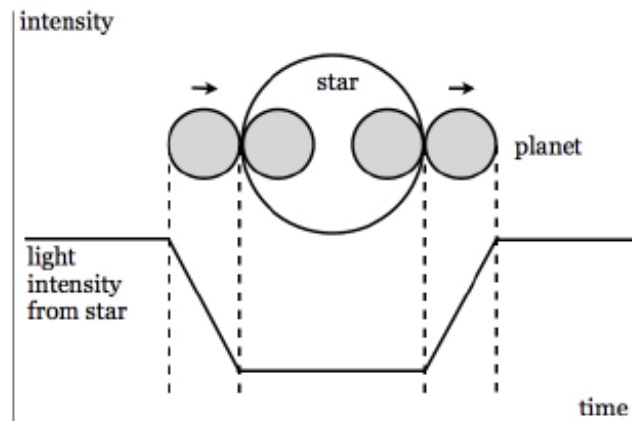


Figure 4.3: Schematic illustration of the transit of planet in front of the star.[18]

Some requirements for this method are raising up.

- A. The instrument detecting the drop have to be sensitive enough to measure changes of luminosity. Less than 1 % for the larger planets, with the order of 10 % of the size of the star and even better sensitivity for smaller planets.

For instance, 0.01 % for the Earth transiting the Sun for the alien observers.

- B. The inclination angle i of the planet's orbit should be very close to 90° for the ground-base observer. It is possible to determine i and radius of the planet too, for the very large planets, that causing huge decrease of the luminosity of the parent star.

The transit method defining the inclination angle can clear up the uncertainties in the mass determination, gained by radial velocity method.

Kepler, the space mission launched by NASA, using transits for discovering exoplanets. In 2014, the new statistical technique "verification by multiplicity" was used. This method partly relies on the logical probability. Since for several stars is very difficult to orbit similarly to each other and stay in stable configuration, the drop of the light is rather caused by planets. Almost 92 % of all discoveries by all methods, that means 745 exoplanets was found by transit detection.

Pulsar Timing

A pulsar, pulsating radio star, is small ultra-dense highly magnetized rotating neutron star. The detection of planets around the pulsar are done by measuring the periodic time changes of the pulse.

The first detection of extrasolar planet was accomplished by Pulsar Timing method as was mentioned in section "Definition and discoveries".

On one hand, timing method can detect planets of the far smaller radii (than any other method can) and at much bigger distance from the pulsar. On the other hand, not many extrasolar planets have been found around pulsar, because the ratio of this objects is very low. Moreover, the high energy radiation of pulsars will not allow to any life form to be created.

Transit-Timing Variation Detection

Transit-timing variation method detect the variations in the timing of transits. Very sensible for observing multiple planetary system with mass of additional star similar to the Earth mass.

Gravitational Microlensing

Gravitational microlensing using the fact that light from distant source is magnified by the gravitational field of the star (lens star) passing close to it or in the foreground. If lens star harbors planet, than it's own gravitational field contributes to lensing effect.

This method is more useful for planets between the Earth and the center of the galaxy, because this part of Milky Way contains very large number of distant stars, that must to be continuously detected for observing the planetary microlensing contribution at an adequate rate.

The advantage of microlensing over the other methods is the sensitivity to detect planets with larger orbits, namely around 1-10 AU away from the Sun. On the other hand, the process of microlensing is non-repetitive, because the justification will occur never again. Moreover, the planet is turn to be more distant, so no additional investigation of properties can be made.

Chapter 4 was done by citations of books [18] and [10].

Chapter 5

Data files from OES

The test data for this thesis is provided by Petr Škoda, a regular staff member of Stellar Department at the Astronomical Institute in Ondřejov. It includes sample file (in FITS format) of the observed object, in this case Beta Lyrae traditionally named as Sheliak, the comparison spectrum (comp), the flat field (flat) and the zero :

c201307040002.fit ⇒ object
c201307040003.fit ⇒ comp
c201307040004.fit ⇒ flat
c201307040014.fit ⇒ zero

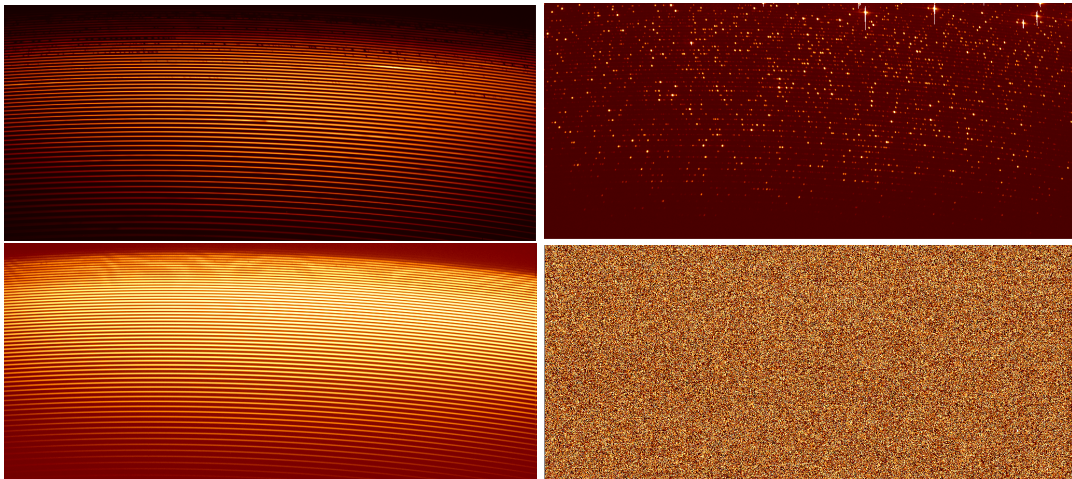


Figure 5.1: Spectrum of star (top–left), comparison spectrum (top–right), flat field (bottom–left) and zero (bottom–right) displayed with ds9.

A comparison spectrum is a spectrum produced by a lamp in laboratory conditions. Thorium-Argon is used in lamp in Ondřejov. Zero or bias belongs to the calibration images. When the spectrograph is closed, without any light, with zero exposure, the CCD camera chip is readout. Flat field images are produced by pointing telescope to the equally illuminated white space. The aim of this procedure is to recognize different sensitivities on the pixels on chip. The exposure time does not necessary need to be equal to the exposure

of the star. Usually, from the flat fields are subtracted the zero images and final the spectrum is usually divided by flat field. Although in case of echelle data this procedure is not possible. Zero is still subtracted, but easy division of the object is not possible in echelle setup. The reason includes the fact that the boundary of orders in cross-section profile of flat are not aligned with those of stellar exposure so after division the strong singularities would appear. Because of this, each order needs to be flat-fielded separately only in 1D extracted spectrum.

Data were produced on 7th of April 2013 in Ondřejov. As it was mentioned in introduction, the OES spectrum shows the tilted spectral lines. This character is obtained in Fig. 5.4. The comparison (Fig. 5.2) of zoomed spectral lines in star spectrum and comparison spectrum is offered. The star spectrum is showing apparent tilt of line, whereas comparison spectrum in the same region only straight lines. This characteristic is explained by the deviation of the spectrograph from a perfect Littrow configuration, which causes spectral lines to tilt. Moreover, the angle varies along each order with position. It is not in IRAF capabilities to deal with those tilts and straighten them. New reduction tool is, therefore, demanded.

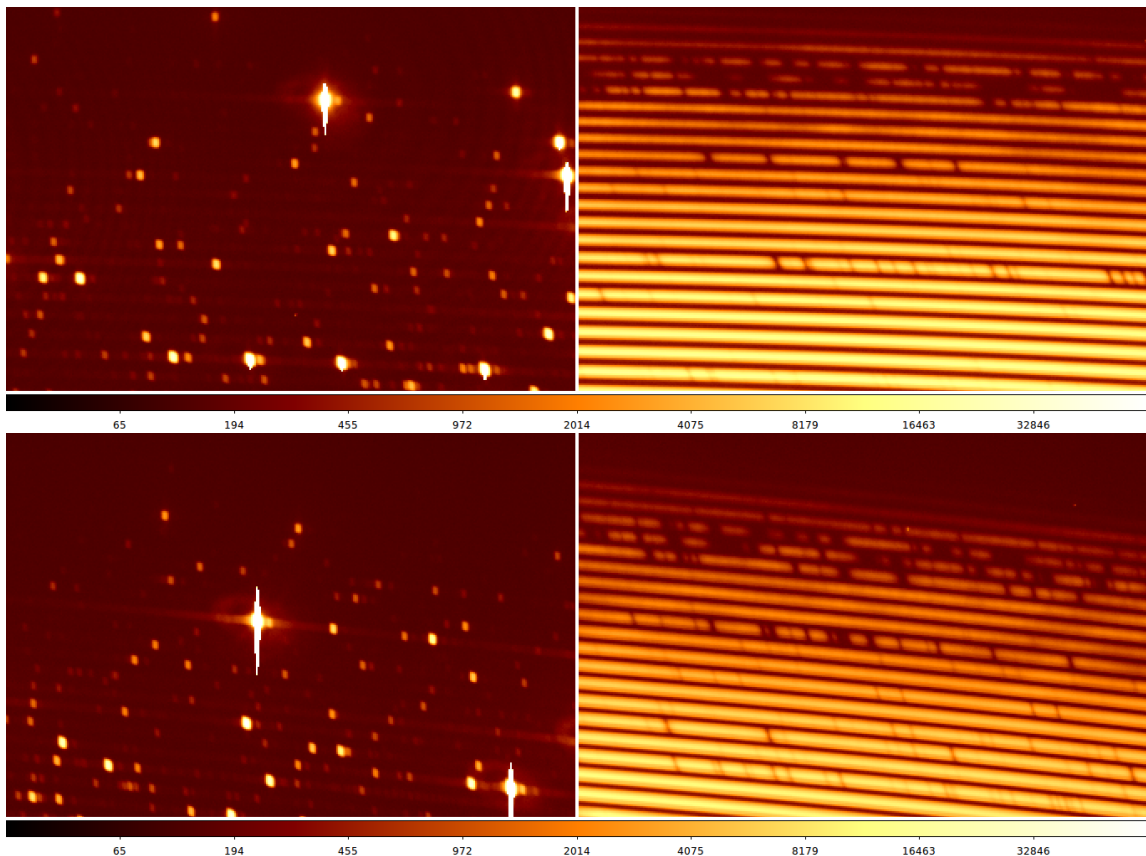


Figure 5.2: Tilt of lines in different part of the spectrum of star beta Lyrae (right) and straight line of comparison spectrum (left).

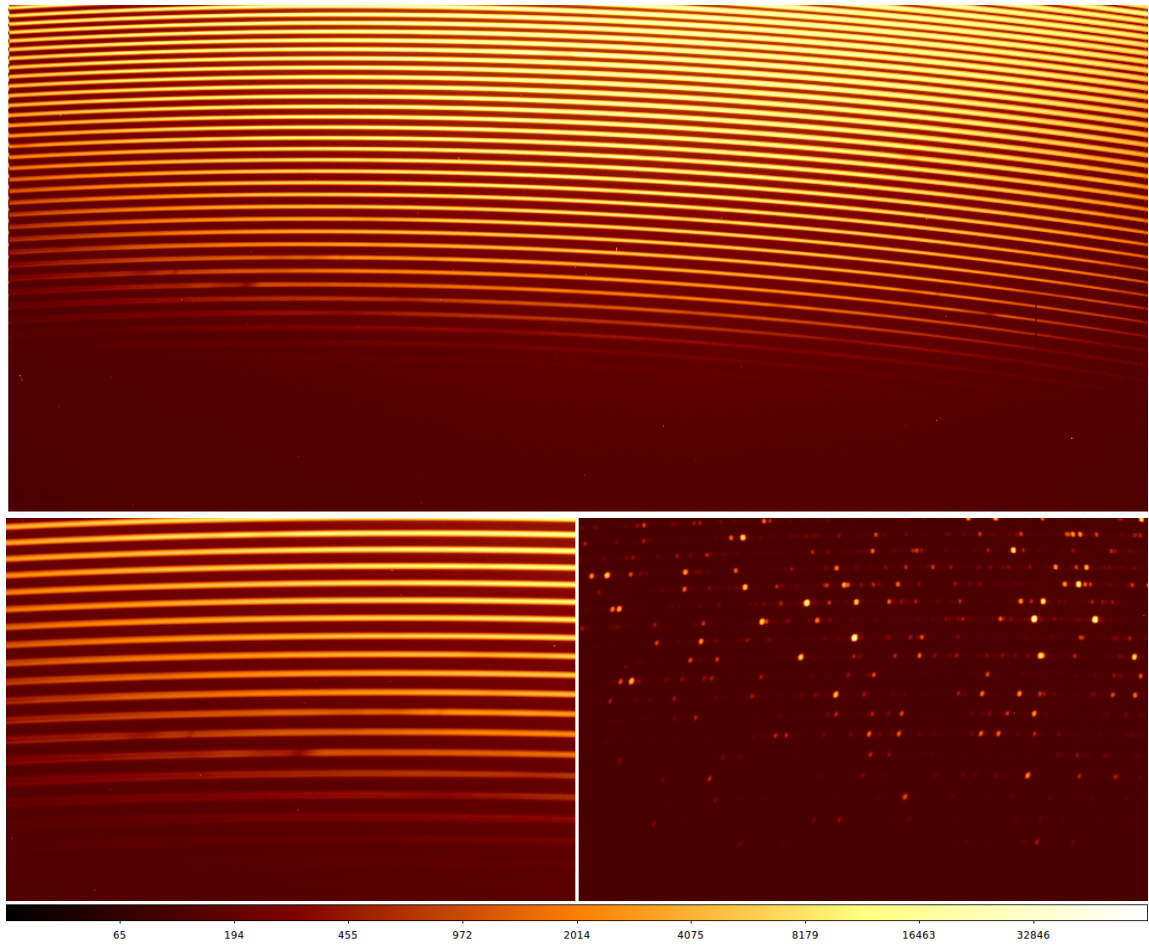


Figure 5.3: Tilt line in blue part of the spectrum of star beta Lyrae (right) and straight line of comparison spectrum (left).

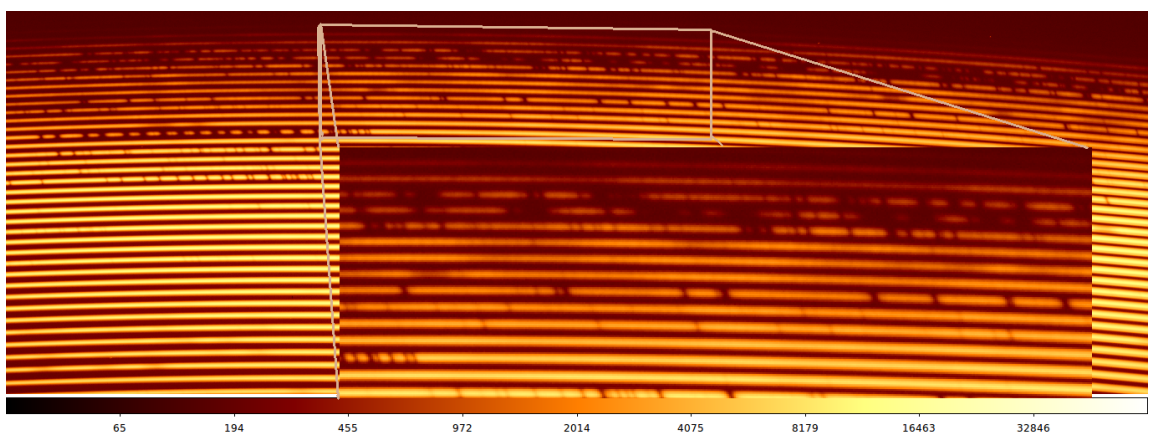


Figure 5.4: Zoomed infra-red part of the spectrum of star beta Lyrae.

Chapter 6

IRAF

6.1 Main Characteristics

IRAF (Image Reduction and Analysis Facility) is the system software project from 80's developed by Peter Shames along with Doug Tody, the chief programmer and the head of IRAF group in the National Optical Astronomy Observatory¹ in Tucson, Arizona. This software was designed to reduce and analyzed scientific data.

Its main capabilities includes reduction of CCD images and spectral data, the detection of the air masses, the calculation of the Julian heliocentric date and the international coordinate system and more and more other.

Although, more that 30 years passed since IRAF was first introduced to the scientific community, it is still one of the most popular software used by professional astronomers.

The latest version IRAF v2.16 was updated on 22. of March 2012 and is freely available for some platforms of GNU/Linux and Mac OSX free of charge. Moreover it comprehends Virtual Observatory (VO) features like URL access to remote data, search in VO data services by the key words, obtain parameters of chosen object and display its images with ds9², load the table to the VO tool for further use, for instance TOPCAT (Tool for Operations on Catalogues And Tables) [22].

Native language of IRAF is SPP (Subset Pre-Processor) a portable pre-processor language which resembles C. [16]

6.2 Installation

The biggest advantage of the new version is simplification of the installation. The problems with the previous versions, I have experienced on my own, while I was working on my bachelor thesis[5]. Back then the installation was difficult in such a degree, that I needed to use functioning version on the server at Stellar Physics Department at Astronomical Institute in Ondřejov.

¹NOAO.

²SAOImage DS9, an application for visualization of astronomical data and displaying images.

The IRAF latest version with the news and updates are available on its websites³ Nevertheless, it is important to download X11iraf⁴ too[23], for graphical support.

Once the IRAF 2.16.1 and X11iraf⁵ are installed and unpacked, the instruction in `~/iraf/iraf/README.install` file is followed. Installation script is dependent on already installed packages, needed for further terminal use of IRAF. The `tsch` enhanced Unix C shell and utilities for terminal use and X11 libraries the `libxss1`, `libncurses5` and `libXmu6:i386` installed as a superuser⁶.

The difference between older version is that there is an global user login file for IRAF command language stored in `~/iraf/login.cl`. It sets the terminal and image type, editors, packages and more. Convenient is to define often used packages by IRAF reduction such as `noao` for optical astronomy packages, the image reduction packages `imred`, `ccdred` and `echelle`.

Moreover, dynamic external packages created in `/iraf/iraf/extern/` directory, can be load and will be automatically define when the program is started. Once again, directions in file is followed.

6.3 Reduction with IRAF

IRAF runs with command `iraf` typed in terminal. Consequently the new window is opened in command line (cl) and ready to fulfill any wishes. Highly recommended for reduction IRAF is the manual by Ch. W. Churchill[6] or by Aoki Wako [19].

The OESPACKAGE pipeline

Petr Škoda produced partly automatic pipeline for reduction of echelle data from the Ondřejov Echelle Spectrograph. This useful tool called `oespackage` and is available on the web of Stellar Department and need to be included into the `/iraf/iraf/` directory. The update of this package was needed, since it was created in 2009 and some updates and arrangements were made on the spectrograph.

Important is the presents of `login.cl`, `coude.dat` to define OES as a default instrument for further analysis with IRAF and to create `loginuser.cl` with the path to this package:

```
set oespath="/iraf/iraf/oespackage/"
task $oes = "oespath$oes.cl"
keep
```

To test if it is all set right, simply run IRAF in this directory with data for reduction, `login.cl`, `loginuser.cl` and `coude.dat`: `iraf`, which opens command line and than type

³Direct link to version for Linux- 32bit:

<http://iraf.noao.edu/iraf/v216/PCIX/iraf.linux.x86.tar.gz>

⁴Direct link for Linux- 32bit: <http://iraf.noao.edu/x11iraf/x11iraf-v2.0BETA-bin.linux.tar.gz>

⁵This package is installed in `~/iraf/iraf/` within all of the README files and RELEASE notes.

⁶`$sudo apt-get install tsh libxss1 libncurses5 libXmu6:i386`

oes. Subsequently all of the oes tasks (including trancoes, traceoes, prepoes, procoes, listoes, and others) should be displayed.

Steps of the reduction

- A. The reduction starts with trancoes task for transforming all files according to x- and y-axis. This process is also adding "t" in front of the file name, for instance the object will be renamed into "tc201307040002.fit".
- B. The directory prepoes is for trimming already transformed images (starting with tc*) to final forms of required size adjusted in order to remain the same as OPERA is using, to trim its images. Since the prepoes is using IRAF's ccdproc tasks, the size can be define by simply changing the parameters in \$ /iraf/iraf/oespackage/ /prepoes.c1/.

```
ccdproc.trimsec=' '1:2048,420:1450"
```

The process is loading the transformed files and allows the previews to check if images are suitable for further process. Different commands offer possibilities to see the head of the file, file information, ds9 image control. By pressing of key ENTER confirms, that certain image of zero, flat or star is suitable for further analysis and first to will be combined.

- C. Along with flat and zero combining the task procoes is also used for the bad pixels corrections. Moreover, this changes can be checked by extracting the information about updated files with command ccdlist, for instance, the information about the object will be:

```
tc201307040002.fit[2048,50][real][object][ ][BTZ],
```

,where real says that the image was already processed, followed by the ccdtype of the image and the last are the letters for corrections on the spectrum.

- D. To trace the apertures and extract the data from 2D CCD image is used traceoes. Concentrating on the update of the oespackage and synchronizing it with OPERA, the reference flat is created by adding the option isnewre+ together with traceoes. Important was to localize start of the aperture corresponding to those for OPERA. The best option was to concentrate on the position of H α in the object spectrum displayed by traceoes. The process is following: undefined apertures of β Lyrae are displayed in interactive window, the aperture comprehending H α is estimated by trail and error at centered location with value ~ 217 and is proved by marking this aperture with m, tracing with t and extracting with e by preview this line should be displayed as shown in Figs. 6.2.

The last picture of this Figure includes final reference flat with define apertures and how it was found out H α was assigned to the order 44 according to OPERA.

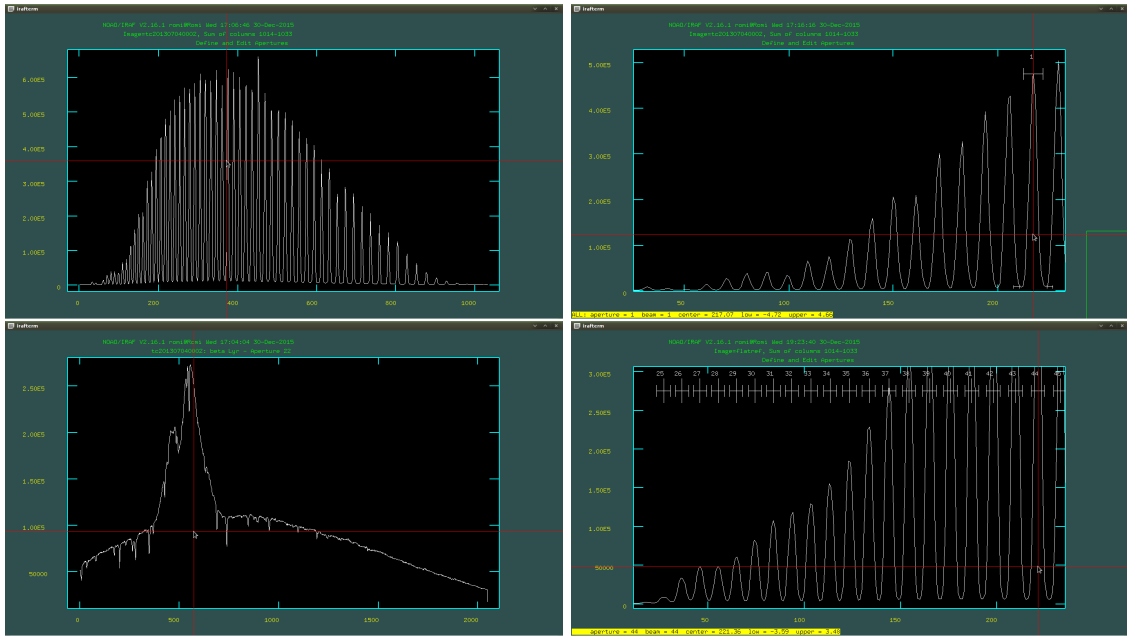


Figure 6.1: Process of defining the numbers of apertures according to those for OPERA.

Apertures need to be found first by pressing `f` in iraf interactive window, followed by command `o 44` for marking the $H\alpha$ aperture, the rest is adjusted by itself starting with 25 and ending with 83. All apertures together are affected after pressing `a` with meaning "all". Consequently, the aperture can be adjusted to certain level for all aperture by commands `:ylevel`, `a` and `z`.

Pressing command `q`, as is standard for IRAF, saves the procedure, after the following questions will arise as confirmation of tracing, writing apertures of reference flat (`flatref`) to the database, extracting apertures and reviewing extracted spectra. Moreover `flatref` is stored in `/iraf/iraf/oespackage/` and will be used as a reference for star, which is edited interactively whereas the comparison spectrum automatically, as define in `traceoes`.

- E. Next identoes is using IRAF's routine for generating a wavelength calibration solution with the list of line wavelengths in calibration lamp exposure, in this case `comp.ec` stored in `/iraf/iraf/oespackage/`, the reference comparison set of thorium-argon lines. Lines were identify manually by using prepared identification of spectral lines within orders starting with 37th up to 81th from the OPERA extractions made by Miroslav Šlechtá and adjusted for identification by Petr Škoda.
- F. Followed by the command `ecidentify`, which identifies the wavelength solution and compare it with reference spectrum. This reference spectrum `comp.ec` is loaded into the interactive IRAF window by `:read comp.ec`. Only one order is displayed at the time, key `k` moves to the next or with keys `:o 37` to 37th order, in case of sample data the first order with identified lines. Reference lines can be shift in contrast with present comparison spectrum. To control current state zooming might be useful, preformed by moving cursor to the lower left corner of part of the image,

that wanted to be examine and using w followed by e afterwards sliding cursor onto the upper right corner pressing key e. The slight shift appears and is solved by pointing cursor onto the center of line that suppose to be marked and using x for cross correlation of the peaks.

To determine how accurate the wavelength solution is enter into the fit mode by hitting the f key. Looking at the RMS residuals to get an idea of the goodness of fit. As recommended in Churchill's manual [6], the fitting should start with the lowest orders and slowly increasing it as long as the sine-shape functional dependence is removed. To improve the fit, points that are obviously incorrect can be deleted by cursor on that point and pressing d. After the residuals are the order of thousandths, leaving the fit mode is preform by q and repeated pressing of this key write the wavelength solution to the database.

- G. Last task preformed automatically is called dispcaloes. The wavelength solution is applied in order to get dispersion corrected spectrum. This command is using as a reference spectrum comp.ec. Important is to define parameter of Ondřejov observatory to the database of all observatories stored in /iraf/iraf/noao/lib/obsdb.dat/, with following parameters:

```
observatory = "ondrejov"  
name = "Ondrejov Observatory"  
longitude = 345:12:59.0  
latitude = 49:54:38.0  
altitude = 528.  
timezone = -1
```

Dispersion corrected spectra are created in following format:

```
> wct201307040002.ec.fit ⇒ beta Lyr  
> wct201307040003.ec.fit ⇒ comp.
```

- H. Heliocentric Radial Velocity Calculation will be preform. The IRAF's rvcorrect computes radial velocity corrections and is using extracted wavelength calibrated spectrum of the star. To preview and adjust parameters load epar rvcor:

```
PACKAGE = astutil  
TASK = rvcorrect  
(images =          ) List of images containing observation data  
(imupdat=          yes) Update image header with corrections?
```

And run this task with ":go" from "epar window", or just save with ":q" and run with:

```
cl> rvcorrect
```

I. Correspondingly, heliocentric correction is applied by task dopcor with output file saved as `wtc201307040002_hc.ec.fit` and `redshift = -VHELIO`.

J. Moreover flat-field can be divided from the extracted spectrum. The task imarit is used to divide final star spectrum and extracted flat file (`Flat.ec`).

Although it seems inappropriate to wait for the division till the end of the process, but it posses crucial reasons for operation like that. Theoretically if the spectrum was adjusted by flat-field at the beginning, that would produce intense peaks and make further analyses more difficult, considering the differences of intensity at the edge each echelle order.

K. Last task scombine is merging multi-order spectra, whereas parameters group and combine can be adjusted [19].

```
PACKAGE = echelle
```

```
TASK = scombine
```

```
(group = images) Grouping option
```

```
(combine= sum) Type of combine operation
```

6.4 Final extracted spectra

Final extracted spectra can be plotted by task splot as demonstrated in Figs. (6.2 and 6.3). Interactive window includes only single order of the spectrum at the time. The move to the next order is accomplished by holding SHIFT key together with pressing left or right parenthesis (or), respectively.

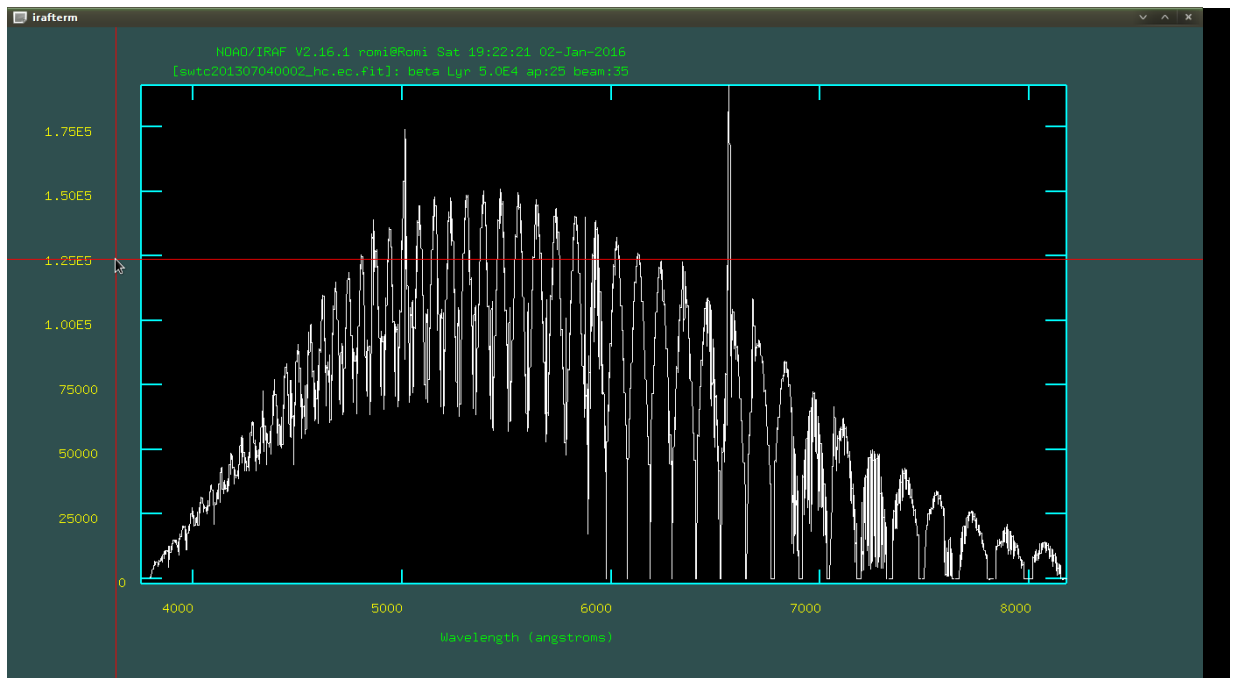


Figure 6.2: Final extracted spectrum for beta Lyrae with IRAF.

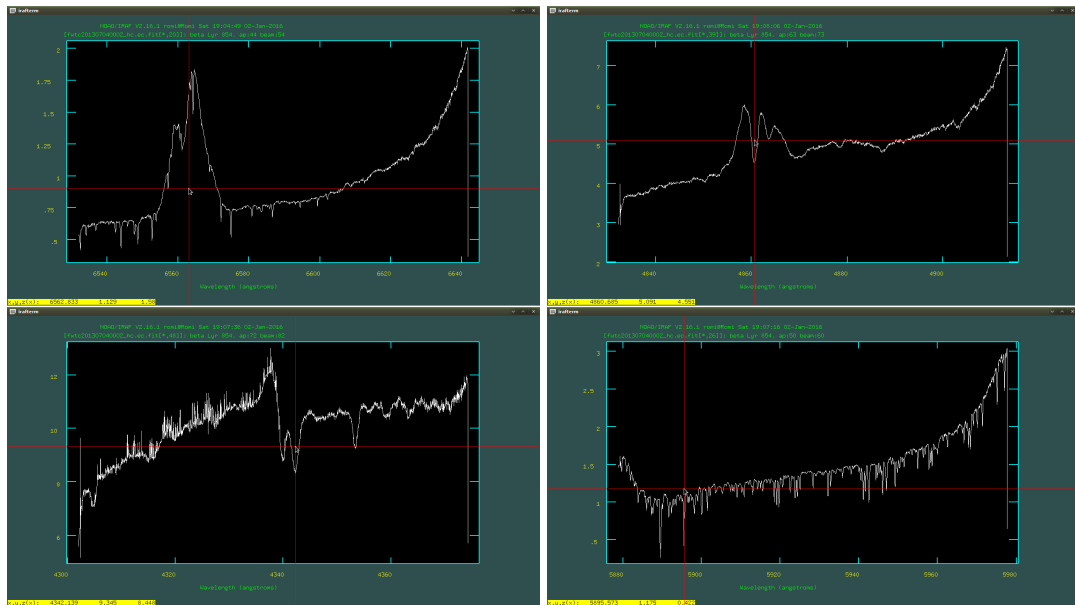


Figure 6.3: Final extracted spectrum for beta Lyrae in different lines with IRAF.

As a matter of fact, final comparison of spectra from OPERA and IRAF is performed in gnuplot. Therefore, conversion of the products from IRAF in ".fit" format to ".dat" files is necessary. Short script was generated for this purpose in Ruby.

First, the script in Appendix B It runs as `ruby iraf_commands.rb 59 wtc20_`, where number 59 defines the last aperture to be processed and second parameter belongs to the input spectrum, that want to be converted.

Consequently, it produces set of lines to extract each order separately with `scopy`, that means one-dimensional files and with `wspectext` converts 1D files to ASCII header followed by data files including two columns with wavelength and intensity.

```
scopy wtc201307040002.ehc.fit[* ,1,1] ly1  
wspectext ly1 ly1.dat
```

Created lines are copied IRAF's command line. Important is to note, that within IRAF's environment is not possible to use customized combination "Copy and Paste", therefore one needs to mark desired lines and to copy them pressing both buttons on mouse together or middle button.

After all pairs of commands are successfully done, second script in Appendix B.1 will look into current directory named as "ly*.dat", load each line of files starting with 143 till the end. To run script and save products to final ".dat" format with ruby `iraf_filter.rb >bLyr.dat`.

This way all files are ready to be examined by `gnuplot`. But first, the comparison data from OPERA need to be produced in next chapter.

Chapter 7

OPERA

In field of data reduction and analysis in spectroscopy arises new powerful tool software pipeline "OPERA". OPERA stands for Open source Pipeline for ESPaDOnS Reduction and Analysis and is an Canada-France-Hawaii Telescope(CFHT) open source collaborative software for echelle spectro-polarimetric data. It is fully automatic and able to performed calibration and reduction of data, produce the one-dimensional intensity and polarimetric spectra and much more. The biggest difference between already existing echelle pipelines in Hawaii should be that OPERA is accessible and adjustable to be used for both GNU/Linux and Mac OSX distributions.

Primary, it is used for data from ESPaDOnS and it is considered to be an replacement for the Upena pipeline using Libre-Esprit software, closed source software developed by Donati in 1995[24]. That was the reason for Douglas Teeple and Eder Martioli to developed an open source software. Eder Martioli is a resident astronomer and part of CFHT Corporation, and Douglas Teeple, his coworker at CFHT is a software engineer.

However, the new statement from CFHT community from October 2015 says, that in 2016 both OPERA and Libre-Esprit will be distributed to the users to get a feedback, before OPERA will eventually take a lead.

7.1 Installation

OPERA pipeline is available on source forge websites¹ [29].

Until the current last version from 7th of October 2015 the process of installation was really difficult followed by many errors and incompatibilities, especially for other than MAC distribution. Codes to run the installation were written in bash scrips with dependencies on ESPaDOnS data. In the half of the year 2015 those scrips were transferred to python by Eder Martioli and also he adjusted them for the OES parameters.

This last available version is downloaded from the source forge websites. Process of installation was preformed on GNU/Linux Mint (my own notebook) and repeated on Debian (on Stellar Astronomy server). Several steps toward successful installation need to be followed and will be demonstrated in next paragraphs.

¹Directed link to download opera-1.0 available on "http://sourceforge.net/projects/opera-pipeline/files/opera-1.0/opera-1.0-Oct07-2015.tar.gz/download"

OPERA package is downloaded and the path to the OPERA is saved in \$OPERA:

```
$ tar xf opera-1.0-Oct07-2015.tar.gz
$ cd opera-1.0/
$ OPERA='pwd'
```

Very important is to concentrate of right version of cfitsio library, the C and Fortran subroutines for reading and writing data files in FITS.

After detailed analysis made by Zdeněk Janák, doctoral student on Masaryk University, was discovered that, last three versions, 3.350, 3.360 and 3.370, are not compatible with OPERA. Problem is in added parameter in those versions, which are slightly different than in OPERA source codes. The use of 3.340 version is chosen and available on NASA websites [30]. This package is downloaded, unpacked, configured and installed as following commands demonstrated:

```
$ tar xf cfitsio3340.tar.gz
$ cd opera-1.0/
$ ./configure --prefix=$OPERA
$ make install
```

Next the OPERA is configured. Specially for OES, calibration files and pipeline running scripts, where added to OPERA and stored in:

```
~/opera-1.0/DefaultCalibration/OES and
~/opera-1.0/pipeline/OES.
```

```
$ cd $OPERA
$ ./configure --prefix=$OPERA --with-cfitsiolib=lib
--with-cfitsioinc=include
$ make install
```

7.2 Wavelength Calibration

Important is to notice, that OPERA was designed and adapted for the needs of ESPaDOnS. Data in input first wavelength guess files for ESPaDOnS (`wcal_ref.dat.gz`) are essential for calculation of wavelength solution with OPERA. This set can be obtain by first identifying spectrum from the Oxygen telluric lines then calculating the model terms:

$$\begin{aligned}\lambda_0(\text{order}) &= a + b/\text{order} \\ \lambda_0(\text{order}) &= a + b/\text{order} + c/\text{order} * \text{order},\end{aligned}$$

where λ_0 is the zeroth order term and λ_1 is the first order term in the pixel-to-wavelength solution. These models calculate λ_0 and λ_1 as a function of order number for ESPaDOnS. Solution are found in module `operaWavelengthCalibration.cpp`.

Although, considering OES the new topic rising up. The linear solution of first guess is not sufficient enough. The new version of OPERA appended an input set of the lines identified manually to the pixel-to-wavelength solution. These lines are used to fit a nonlinear initial solution, which is good enough to detect and identify other lines and converge on a solution using the current algorithm.

Manual identification

The task is clear. Generate file using OPERA script to extract each order separately² and compare it to the Lovis Pepe Thorium-Argon line atlas for assign to each pixel appropriate wavelength.

For the first part is used module *operaWavelengthCalibrationTool* . Files are generated in format for instance "OES_ord39.dat" and plotted with gnuplot ready to further analyses. New gnuplot window is used to plot certain range corresponding to for instance wavelength range of 39th order in Lovis Pepe atlas. Fig.7.1 demonstrates the whole process. The top window shows generated lines in 39th order, pixel to intensity dependency, whereas on the window below wavelength dependence of thorium-argon lines is displayed in range 720-730nm .

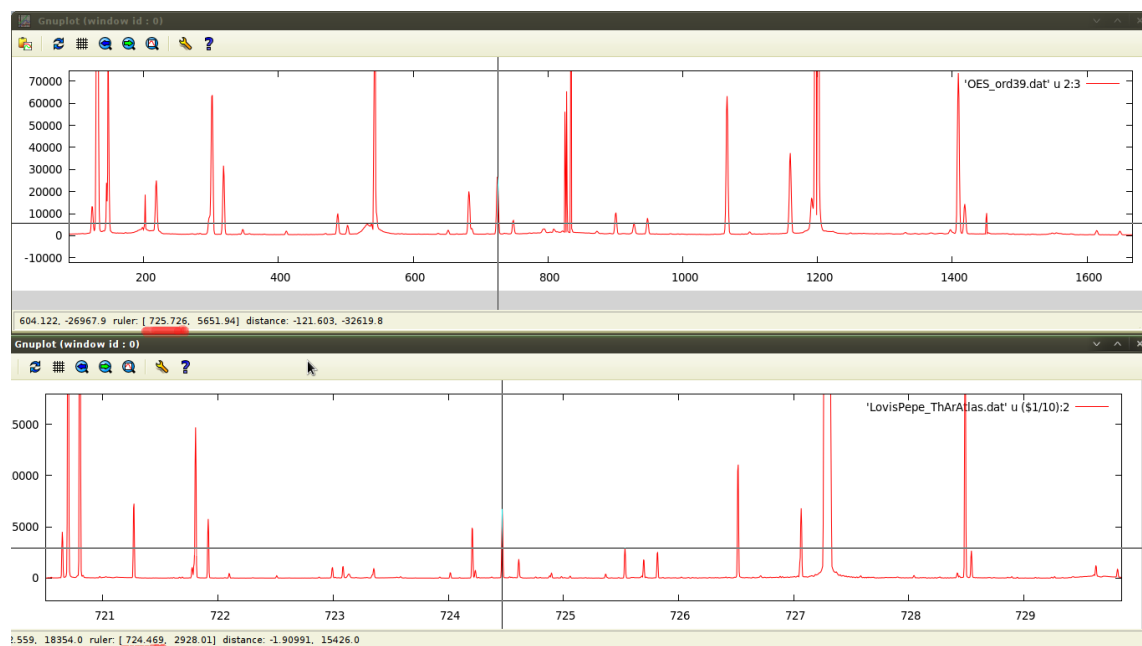


Figure 7.1: Comparison of lines in Lovis Pepe atlas and lines generated for star.

Extremely important is to precisely and responsibly identify the same lines in both gnuplot windows. The values of this lines are determined by pointing the cursor on chosen line and pressing "R" letter on keyboard to fix it on position. In red underlined numbers represent the coordinates, pixels in upper window and wavelengths below. This parts of the coordinates are forming data file "OES_ThArLines.dat". Fig. 7.2 demonstrates data file for order 39 composed of three columns: order number, wavelength in nm and

²this extraction does not include wavelength calibration

distance in pixel. Moreover, created file need to be stored in default calibration directory for OES within opera-1.0³. It is essential for successful extraction of any spectrum of a star observed by OES.

```
OES_ThArLines.dat X
# E. Martioli, LNA -- Dec 14 2015
# List of Th-Ar lines identified manually
# The reference Th-Ar spectrum is LovisPepe_ThArAtlas.dat
#
# ordernumber wavelength[nm] distance[pix]
#
39 720.004 25.3126
39 720.181 52.7661
39 720.252 63.1259
39 720.647 123.731
39 721.668 279.917
39 721.692 283.635
39 721.915 318.988
39 722.098 346.642
39 722.993 487.605
39 724.020 652.381
39 724.469 725.359
39 724.616 748.404
39 725.535 901.269
39 725.701 928.476
39 725.820 947.621
39 727.067 1159.23
39 728.542 1418.17
39 729.813 1649.23
39 730.865 1844.96
39 731.599 1986.75
```

Figure 7.2: Part of the data file created for wavelength calibration.

7.3 Reduction steps

With produced data file, the final reduction step can be followed.

Fully-automated OPERA is hiding several calibration steps. Firstly the calibration creates an calibration images, bad-pixel masks, pixel-to-pixel sensitivity map, geometric and instrument profile, aperture and wavelength, to calculate gain and bias followed by reduction for extraction of intensity and polarimetry. Although, OPERA is fully automatic each step of calibration can be performed individually. All of products are in plain-text gzipped format.

Whereas the reduction includes optimal intensity extraction followed by signal-to-noise calculation, normalization, wavelength telluric correction and creation of final product with extension `*spc.gz`.

Data files are the same as were used by IRAF reduction in previous section and store in created directory:

`~/testOES/data/`.

The products can found in

`~/testOES/REDUCED/`.

³`~/opera-1.0/DefaultCalibration/OES/`

The reduction is run by the python script `operaoes.py` and next the paths to directories are set.

```
$ /homedir/opera-1.0/pipeline/OES/operaoes.py
--datarootdir=/homedir/testOES/data/OES/
--pipelinehomedir=/homedir/opera-1.0/
--productrootdir=/homedir/testOES/REDUCED
--night=2013-07-04
--product="OBJECTS" -pvt
```

The last parameter `--product` defines, what will be produced. Several options are possible such as a "CALIBRATION" or anything from procedures that OPERA is offering: "GEOMETRY", "INSTRUMENTPROFILE", "WAVELENGTH", "EXTRACT", etc. In any of these cases it will produce all the dependencies before it gets to the final desired product. At last, the options `-pvt` are set and described the produced plot files `-p` parameter, for instance `*eps`, `*dat` or `*gnu`, required by gnuplot, `-v` for verbose and `-t` for printing command lines. Useful testing option is offered too. Including parameter `-s` runs the simulation of the process. This means it will only print out all command lines on the screen but will not execute anything. It is very useful for testing the steps of calibration and reduction.

After successful complete extraction of final spectra, in product file are created several important files:

A. Plots for geometry calibration:

```
>2013-07-04_OESBLADE_100kHz_spcplot.eps
>2013-07-04_OESBLADE_100kHz_geomplot.eps
```

Opera geometry calibration contains detection, tracing, enumerating of spectral orders and the order of center points from master flat-field image. The output can be found in `*.geom.gz` with the order of polynomial for each order, the polynomial coefficients and coefficient errors.

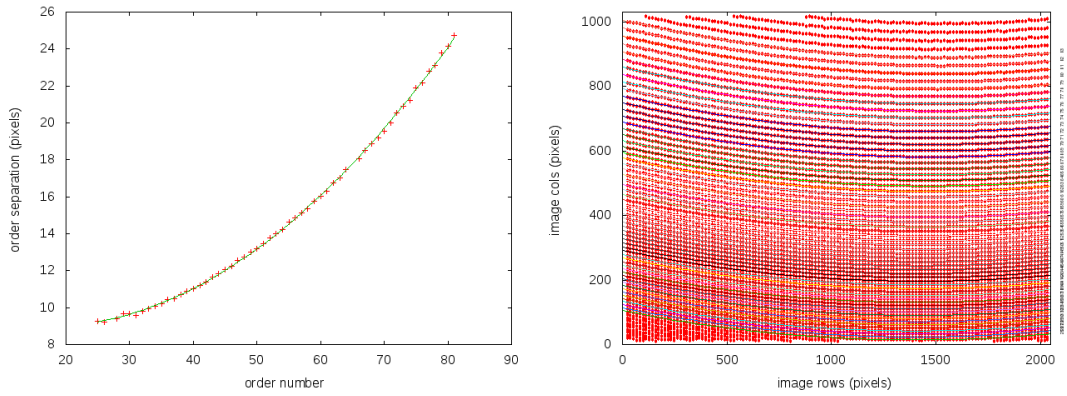


Figure 7.3: Output geometry calibration plot from OPERA.

B. Plots for the instrument profile calibration:

>2013-07-04_OESBLADE_100kHz_profplot.eps

>2013-07-04_OESBLADE_100kHz_aperplot.eps

This part of calibration measures two-dimensional over-sampled normalized instrument profile as a function of image coordinates at the given size and setting up and calibrating the aperture for extraction with previous module to measure the orientation of a given slit. The users can select a number of beams to divide the slit into independent flux measurements as a result of rectangle shape of this slit. Module also creates two additional smaller apertures on both sides of the slit for background estimates.

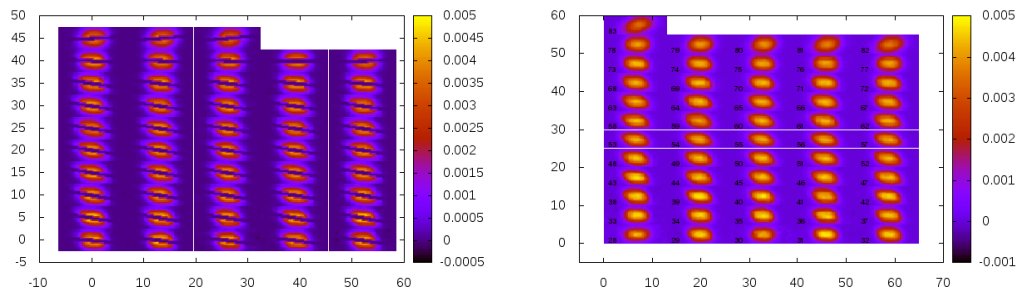


Figure 7.4: Output profile (right) and aperture (left) plot from OPERA.

C. Wavelength calibration solution plots:

>2013-07-04_OESBLADE_100kHz_waveordsplot.eps

>2013-07-04_OESBLADE_100kHz_wavespecplot.eps

Waveleght calibration is used to detect spectral lines and comparing them with the lines of specific lamp. Usually is used Th–Ar atlas. In the beginning it takes a set of known spectral lines from reference atlas and matches it against lines measured from comparison image as the highest correlation between those lines. Then module stores vector of wavelengths in nm and distances in pixels for identified lines and an optimal polynomial is fit to model data

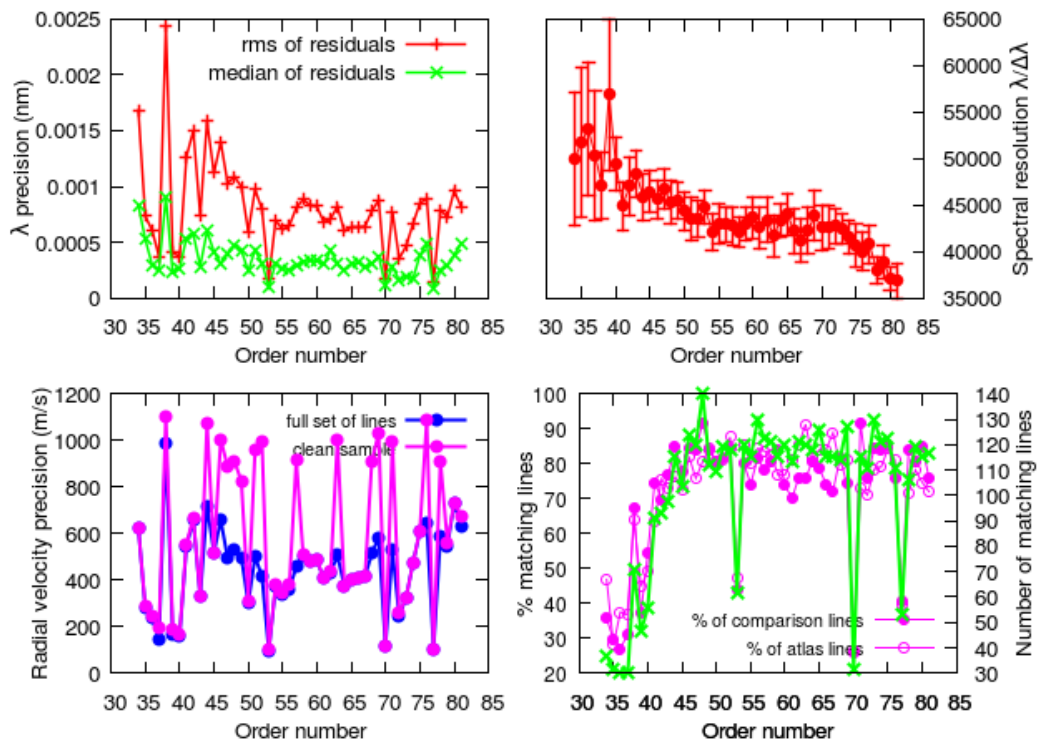


Figure 7.5: Output wavelength solutions plots from OPERA.

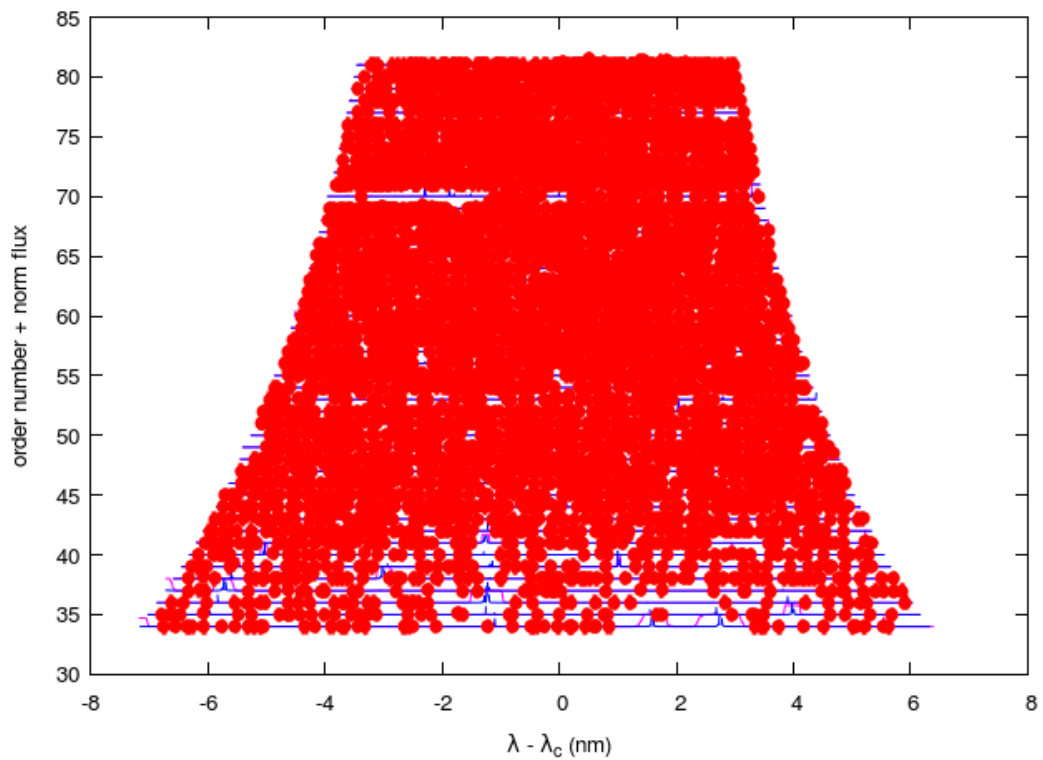


Figure 7.6: Output wavelength solutions plots from OPERA.

D. The raw extracted spectrum of the comparison lamp:

>2013-07-04_OESBLADE_100kHz_comp.e.gz

E. The raw extracted spectrum of the flat field exposure:

>2013-07-04_OESBLADE_100kHz_flat.e.gz

F. The raw extracted spectrum of the object:

>c201307040002.e.gz

G. The reduced spectrum of the object:

```
>c201307040002.spc.gz4
```

The description inside of the file `c201307040002.spc.gz` comments the meaning of each column. Interest is put on 5th column with wavelengths, 9th with raw flux, 11th containing normalized flux and 13th for flux of spectrum divided by flat-field. In order to produce whole final spectrum and in $H\alpha$ as demonstrated in Fig. 7.7 and 7.8, first it needs to be unpacked with:

```
$ gunzip c201307040002.spc.gz
```

and then following gnuplot script in Appendix A produces output image.

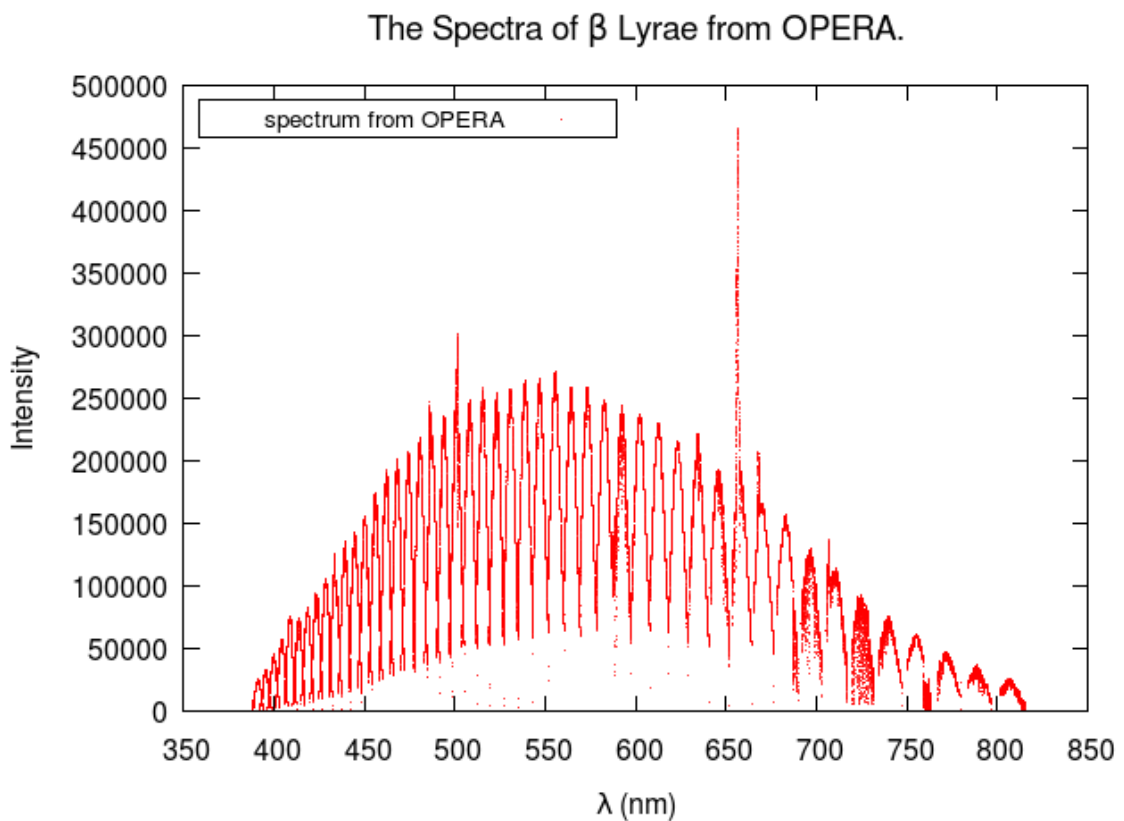


Figure 7.7: Extracted spectrum of the star beta Lyrae.

⁴Note, that all produced files described above are text files with headers including the basic information about the products.

The Spectra of β Lyrae: H α .

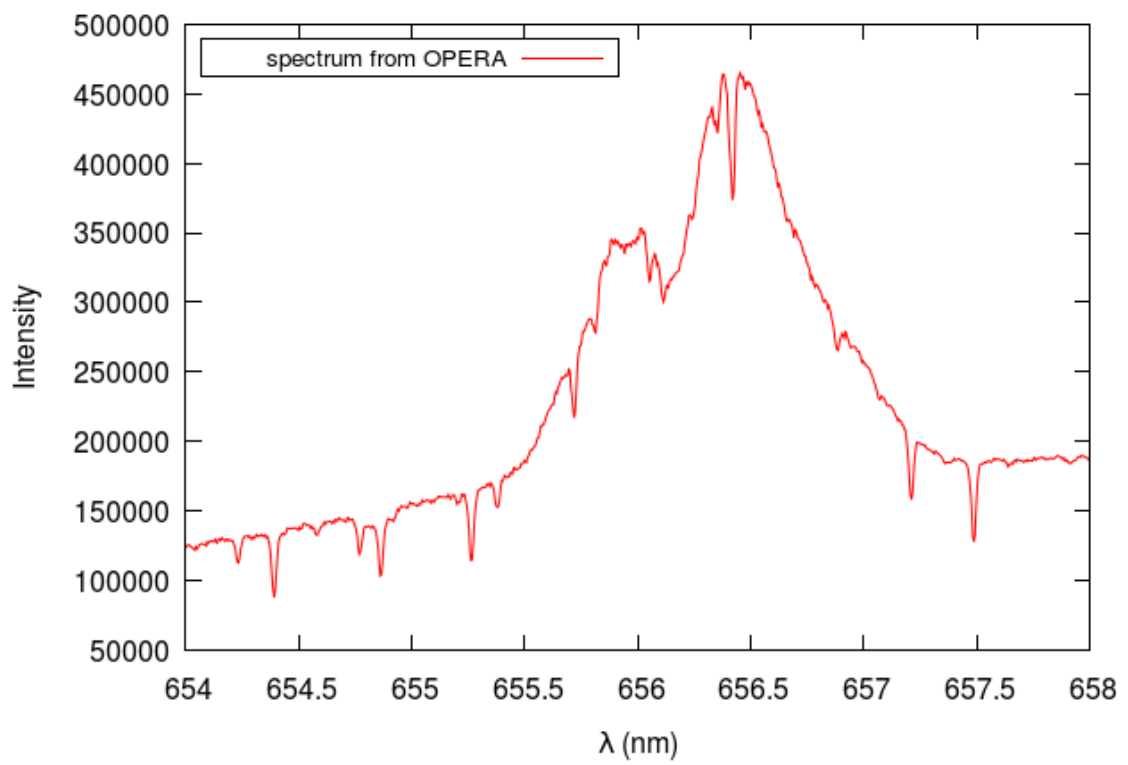


Figure 7.8: Zoom on H alpha in extracted spectrum of beta Lyrae.

Chapter 8

Comparison of spectra from OES

In this chapter will be perform the comparison of final spectra from OPERA and IRAF. Several gnuplot scripts were written in order to gain higher effectivity and are available in Appendix [A](#).

All spectra in this chapter were corrected by heliocentric correction, although Fig. [8.6](#) shown that the spectrum extracted by OPERA is sightly shifted in comparison to the others from IRAF. It might be the problem of some missing parameter in OPERA extraction, causing wrong calculation of heliocentric correction. Further analysis will be applied.

Beta Lyrae

At first the spectra of the star from our sample data, beta Lyrae, are compared in gnuplot. Fig. [8.1](#) and Figs. [8.2](#) illustrate the whole raw extracted spectrum and flat-field extracted spectra for three lines of Balmer serie and Sodium doublet.

Titled spectral lines

The problem of the tilted spectral lines for OES (Chapter [5](#)) unsolvable only for IRAF, has the effects on the near infra-red part of the spectrum for β Lyrae. Considering the wavelengths in the range 802-815 nm effects on stellar lines are visible in comparison with stellar lines from OPERA reduction. Such case is depicted in the following Fig. [8.3](#).

The Spectrum of β Lyrae.

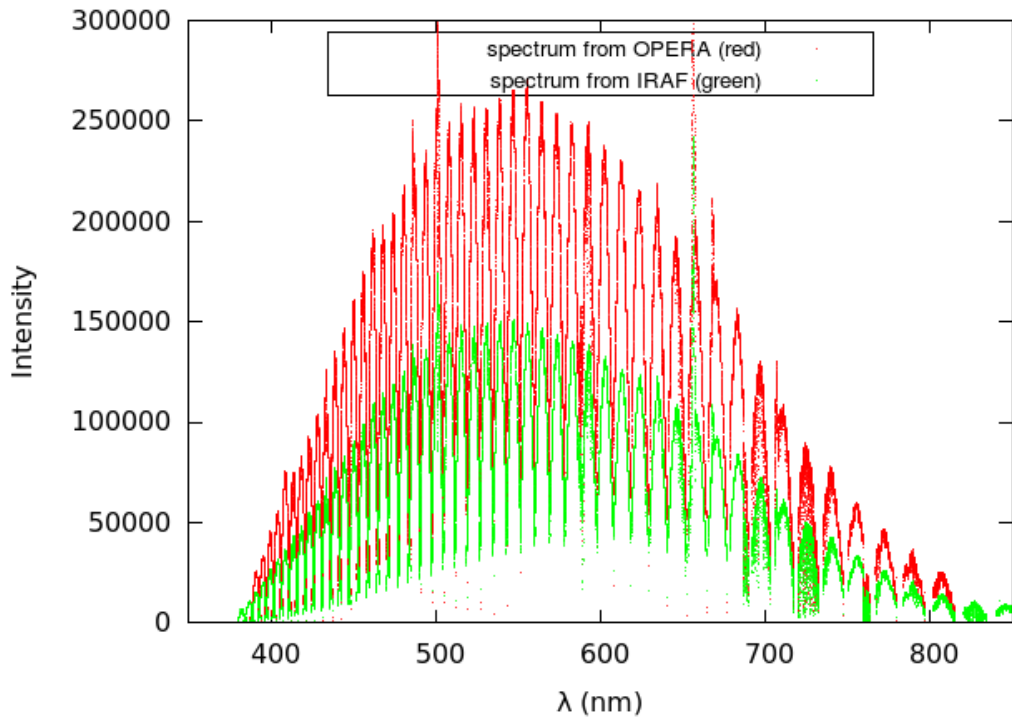
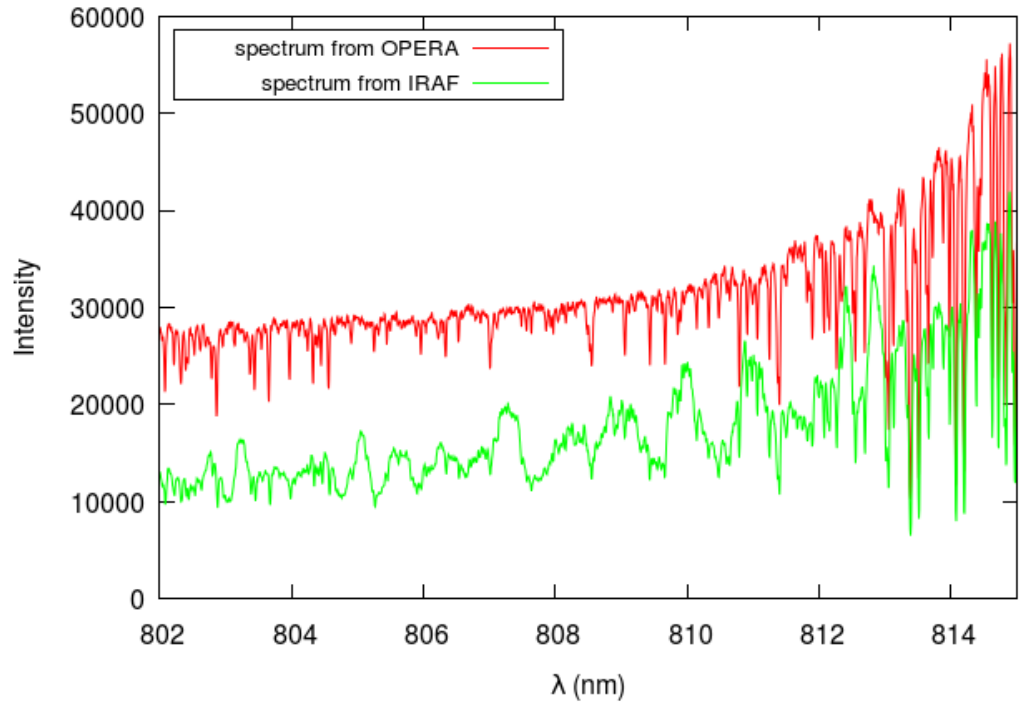


Figure 8.1: Extracted spectrum of the star beta Lyrae.



Figure 8.2: Extracted spectrum of the star beta Lyrae .

The Spectrum of β Lyrae in near infra-red.



The Spectrum of β Lyrae in near infra-red.

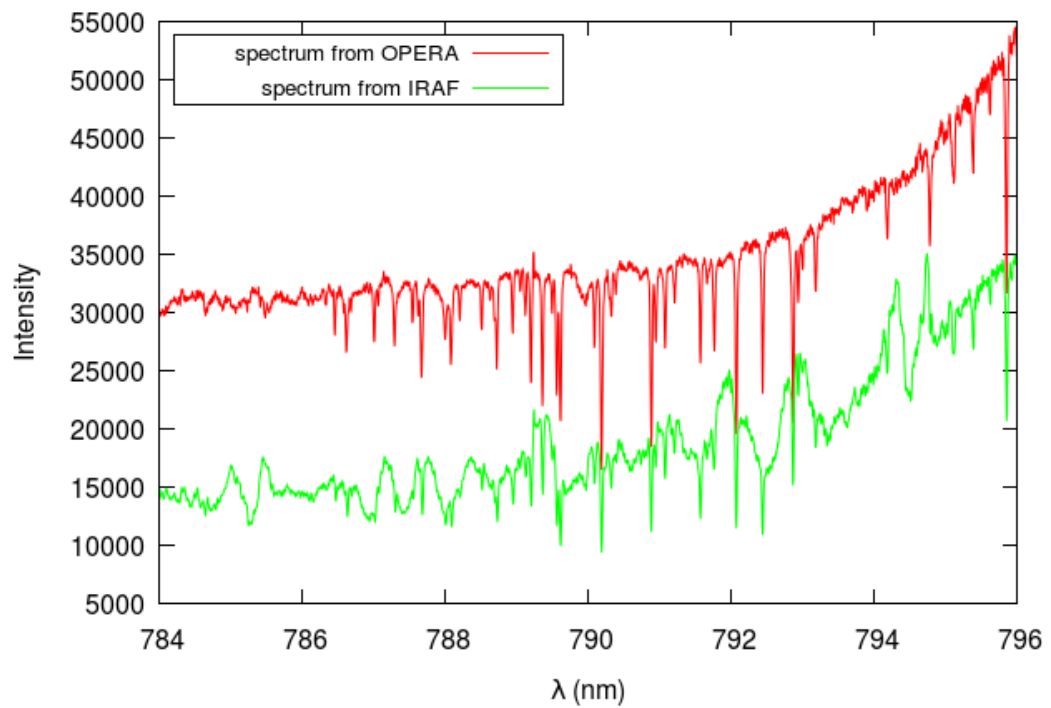


Figure 8.3: Result of tilted spectral line in spectrum of beta Lyrae.

Epsilon Aurigae

Data from OES observed 30th of August 2015 by Miroslav Šlechta from Stellar Department of Astronomical Institute in Ondřejov. The final spectrum of the star epsilon Aurigae, also known as Almaaz, located slightly below Capela in Auriga constellation is displayed in Figs. 8.4 and 8.5. Comparison of spectra from both pipelines is shown.

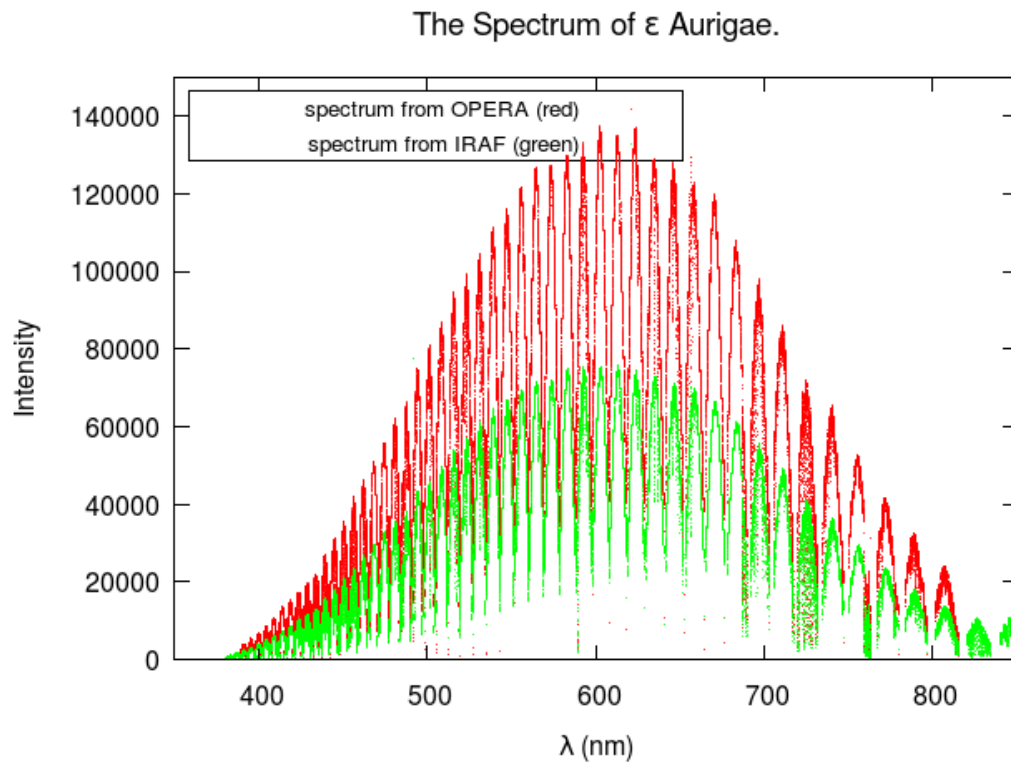


Figure 8.4: Extracted spectrum of the star epsilon Aur.

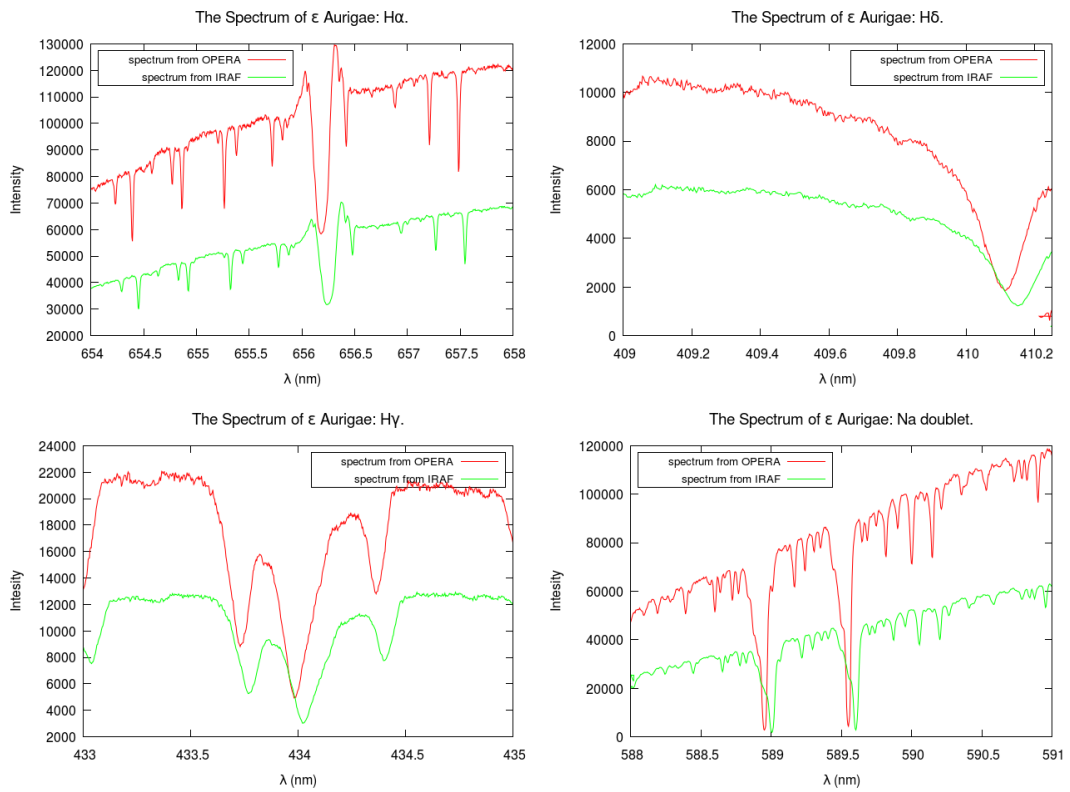


Figure 8.5: Extracted spectrum of the star ϵ Aurigae .

Standard versus echelle spectrograph

Miroslav Šlechta observed ϵ Aurigae on 30th of August not only with echelle but also standard spectrograph (CCD 700). The results in H α of comparison extraction in OPERA and IRAF for echelle and in IRAF for standard are shown in Fig. 8.6.

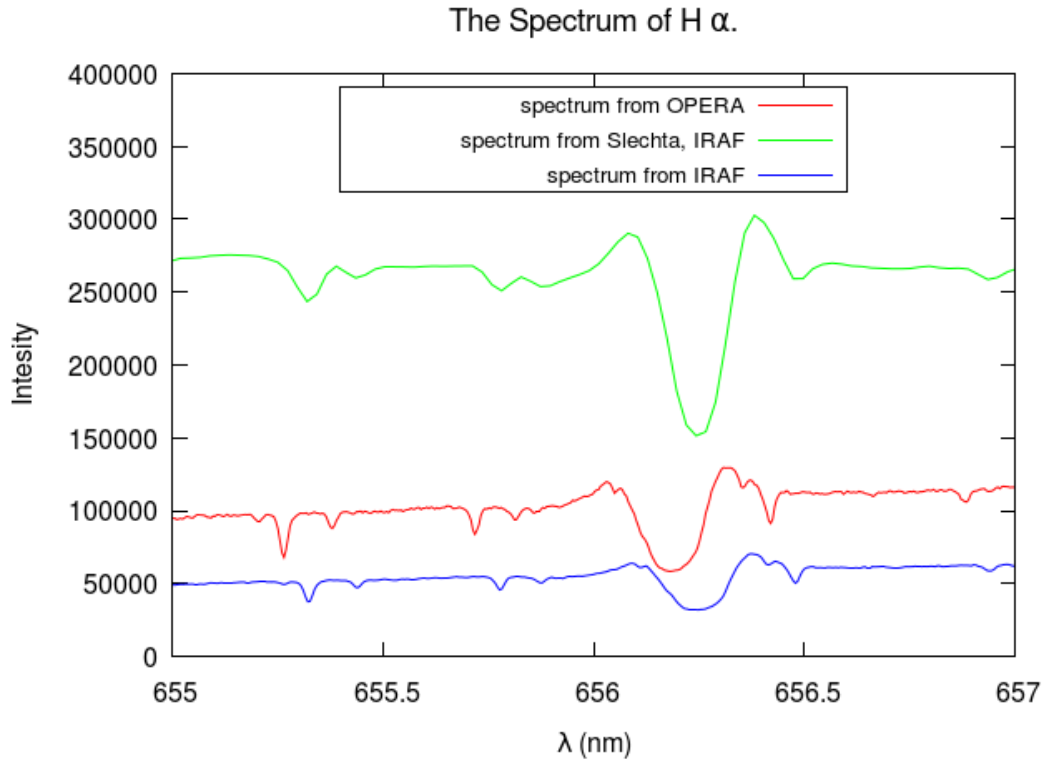


Figure 8.6: Extracted spectrum of the star ϵ Aurigae.

Alpha Canis Minoris

In April 2015, alpha Canis Minoris, Procyon was observed. The whole spectrum together with Na and H lines of this F-type star are plotted in Figs. 8.7 and 8.8.

The Spectrum of α Canis Minoris.

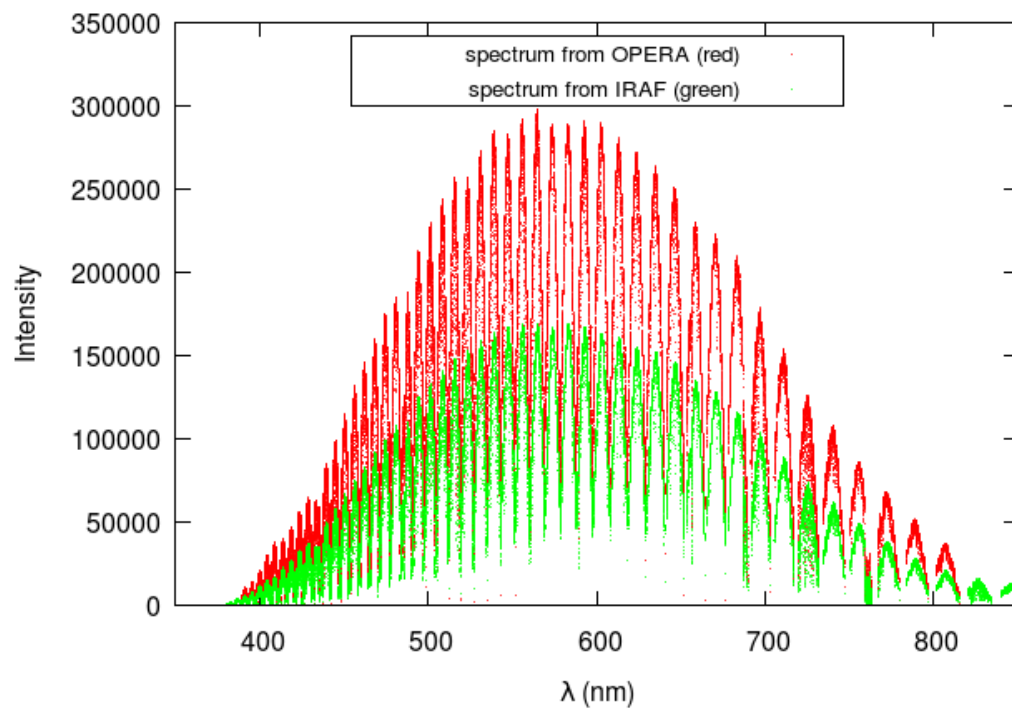


Figure 8.7: Extracted spectrum of the star alpha Canis Minoris.

Overlapping orders

An example of overlapping orders around blue part of spectrum gives Fig. 8.9. On the other hand, in OES echelle spectrum from 600 nm orders start to be separated. This is illustrated in Fig. 8.10.

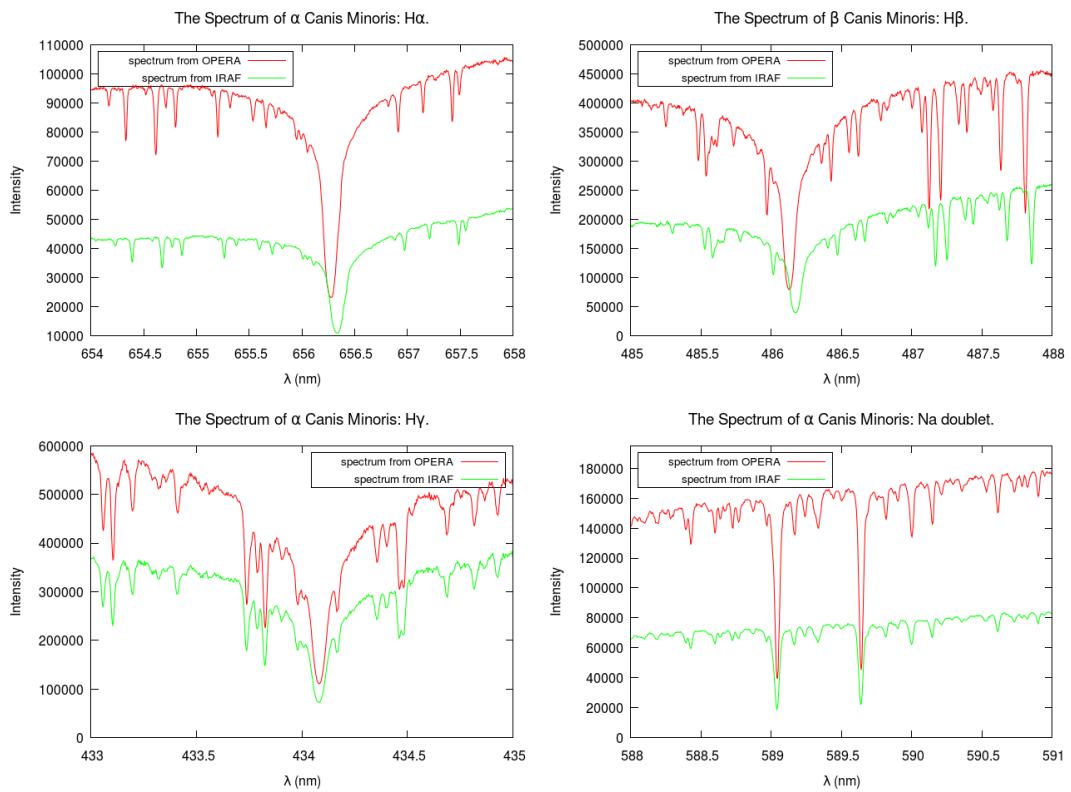


Figure 8.8: Extracted spectrum of the star alpha Canis Majoris .

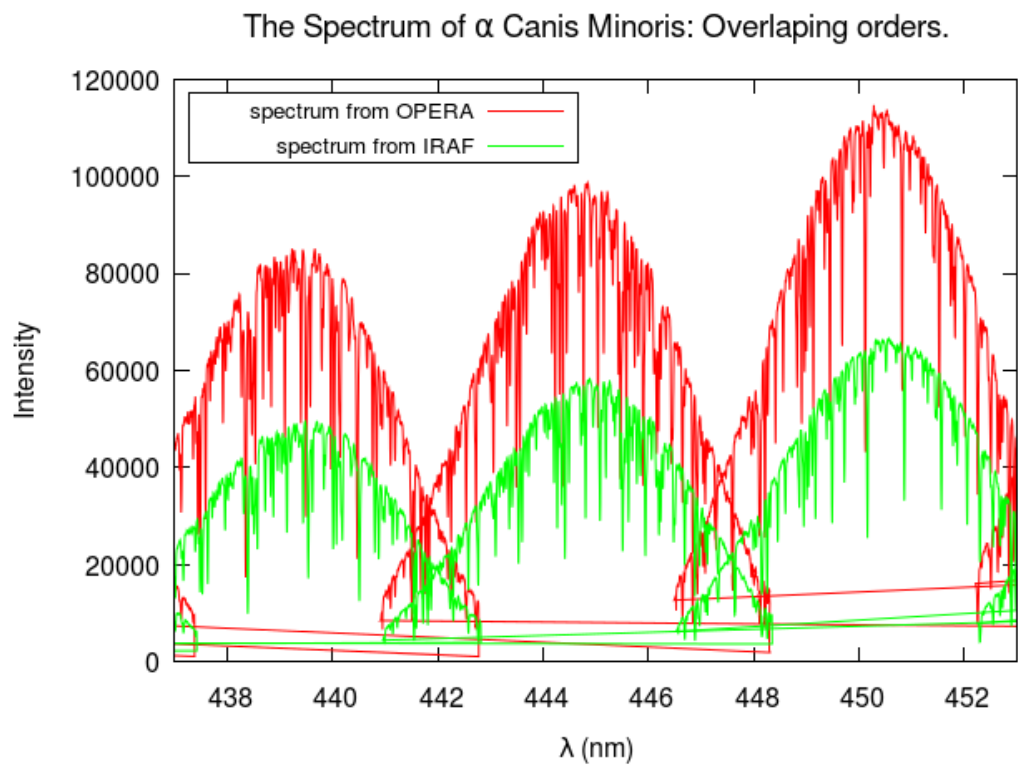


Figure 8.9: Overlapping orders of spectrum of the star alpha Canis Minoris.

The Spectrum of α Canis Minoris: Not overlapping orders.

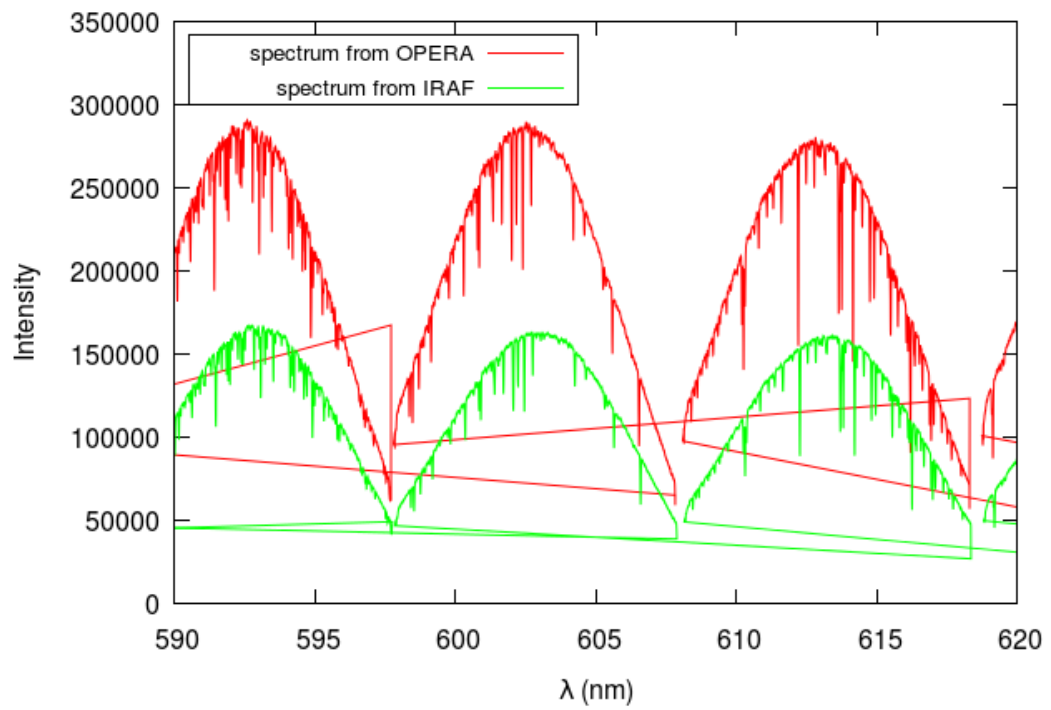


Figure 8.10: Orders do not overlap at the wavelength 600 nm anymore.

Eta Ursae Majoris

The same night were exposed much more stars than only α CMi. Observations of the most eastern star of constellation Ursae Majoris, η UMa took a place during this night too. Traditionally named Alkaid is much more hotter star than α CMi corresponds to the width of its lines plotted in Fig.8.11.

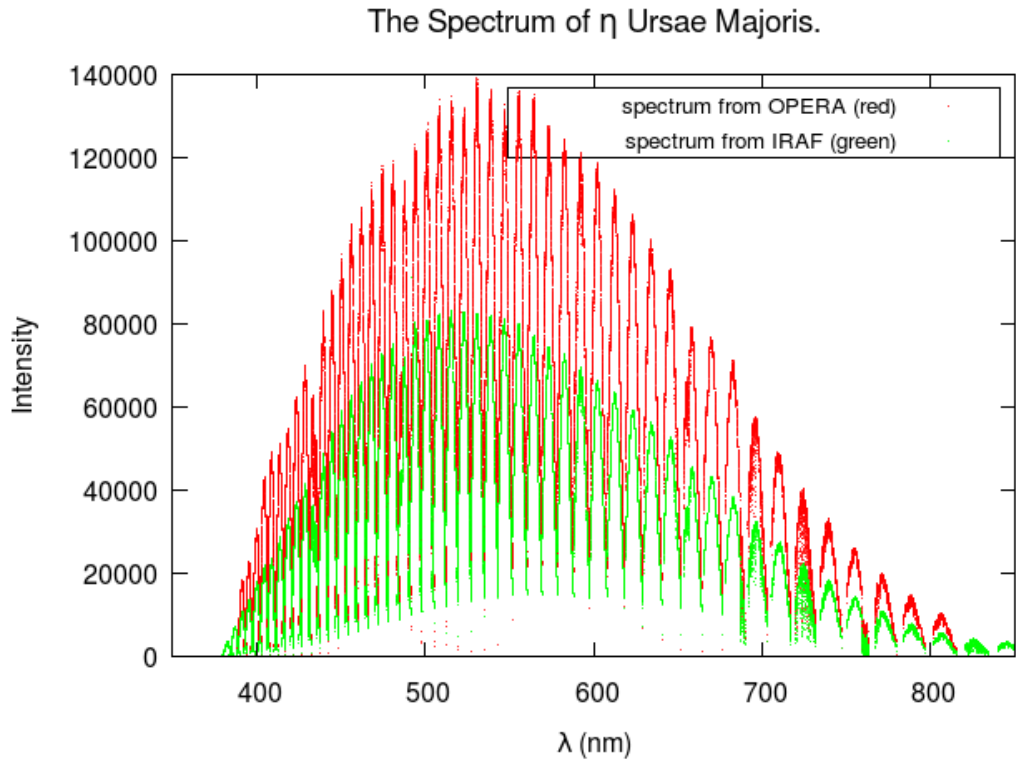


Figure 8.11: Extracted spectrum of the star eta Ursae Majoris.

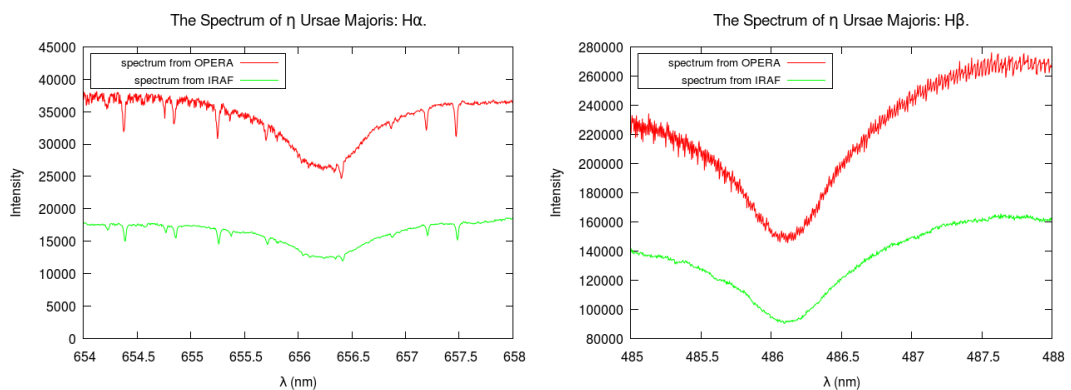


Figure 8.12: Extracted spectrum of the star eta Ursae Majoris.

Spectra with Iodine cell

As it was noted in the Chapter 3.1, Ondřejov echelle spectrograph has an Iodine absorption cell. Sample data observed with and without Iodine cell are presented in this section. As is shown in Figs. (8.13, 8.14 and 8.15) spectra exposed with iodine cell contain considerably more lines, evoke the feeling of spectrum suffering from noisy signal. However, as mentioned before it is just dense forest of absorption lines in range between 4800 Å and 6100 Å .

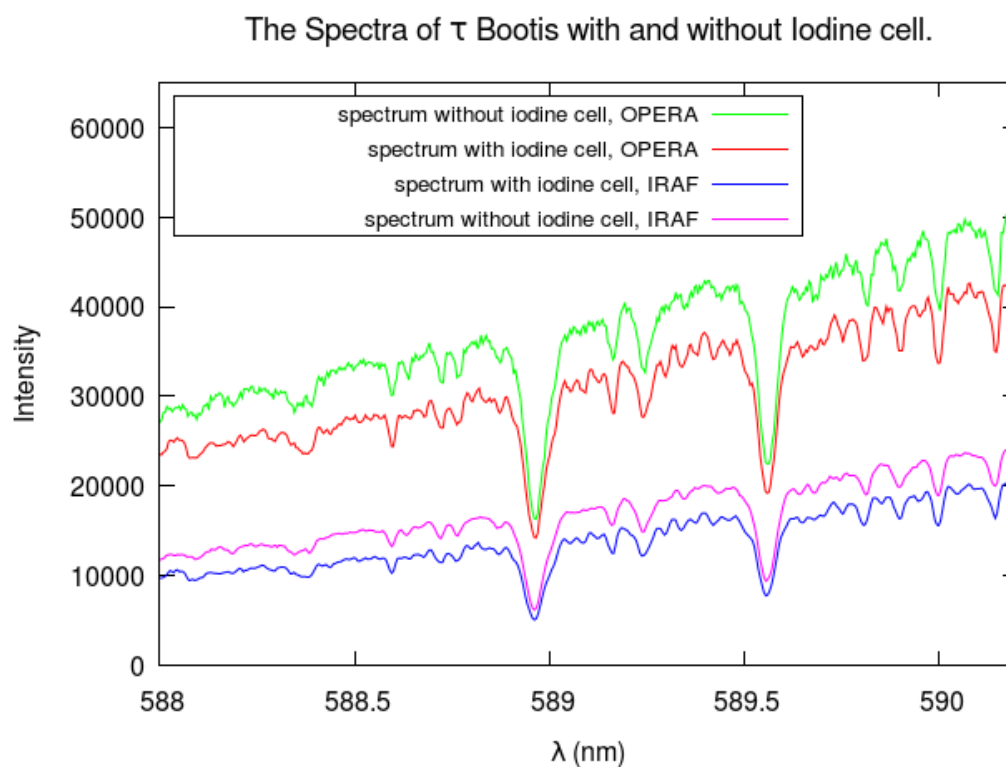


Figure 8.13: Extracted spectrum with and without Iodine cell.

The Spectra of τ Bootis with and without Iodine cell.

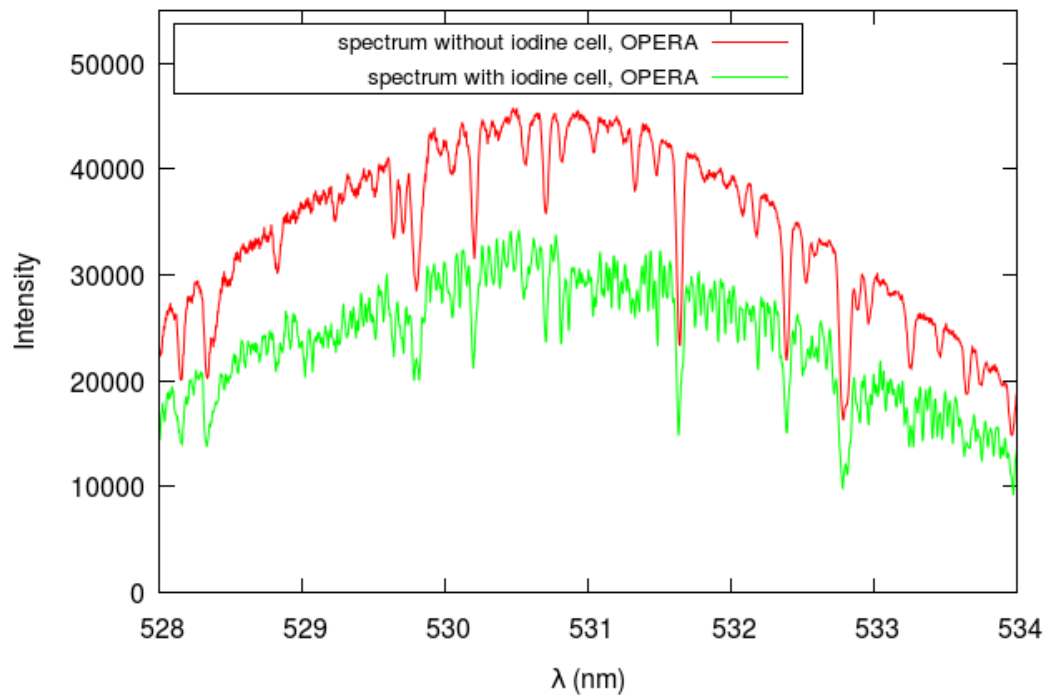


Figure 8.14: Extracted spectrum with and without Iodine cell zoomed in green part.

The Spectra of τ Bootis with and without Iodine cell.

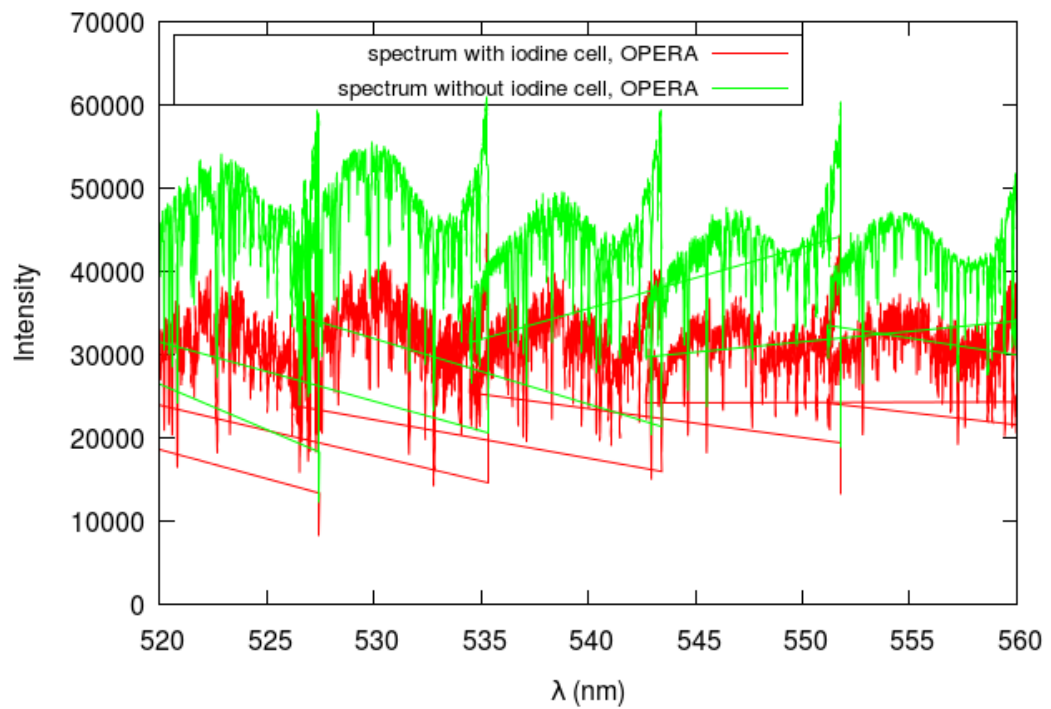


Figure 8.15: Extracted spectrum with and without Iodine cell in range of the highest absorption of Iodine cell.

8.1 Spectrum of stars in H α

Last spectrum presents spectra of different stars in astronomically important line, Hydrogen, from the 9th April 2015. Spectrum was calibrated that night for σ Drakonis, τ Bootis, α Canis Minoris and η Ursae Majoris. In the Fig. 8.16 the hottest star, spectral type B3 V, of this sample is represented by broad H α line. Because of the fact that this line has different value of radial velocity for each star, the lines are not fitting on each other.

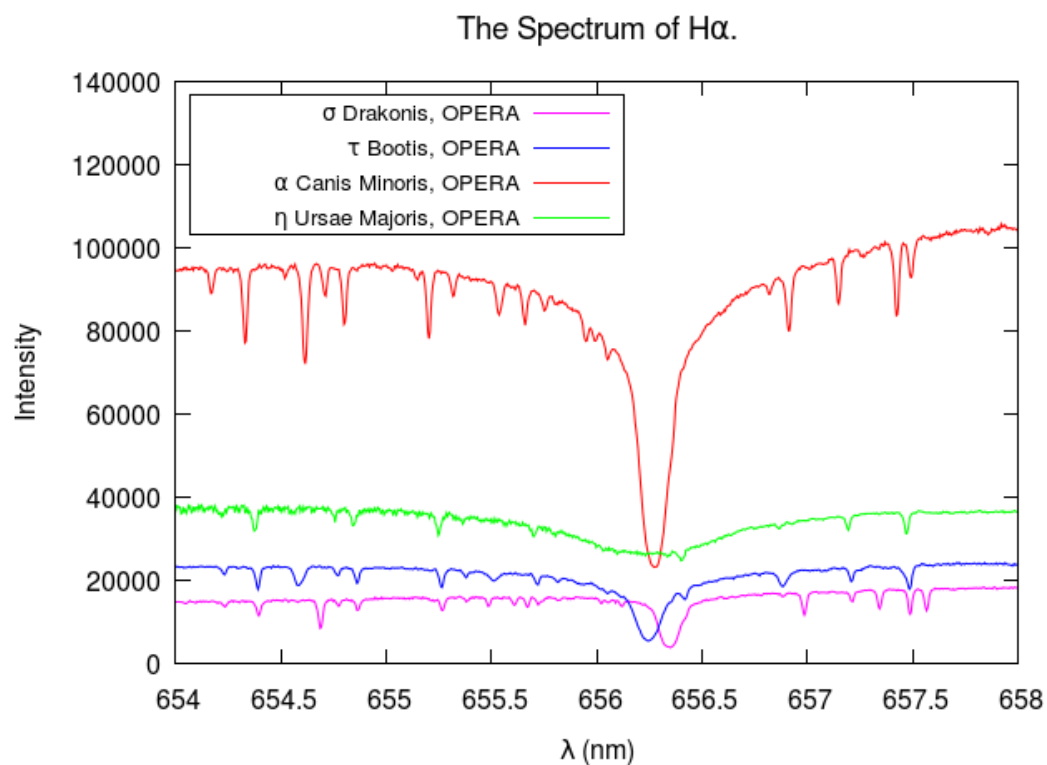


Figure 8.16: H α in spectrum of different stars from April 2015.

Chapter 9

Summary

In this thesis was the analysis of different reduction tools in spectroscopy conducted. The software was produced in 80s, but still often used by wide field of astronomical community. Even this popular tool called the Image Reduction and Analysis Facility, IRAF, has its weaknesses. In other words, it is suitable for any kinds of reduction a analysis of astronomical data, except data from OES, Ondřejov Echelle spectrograph. The main reason is the problem of tilted spectral lines with respect to echelle orders widely present in spectra of OES. Because IRAF does not include any tool dealing with this problem, it is not the perfect choice for data analysis of echelle spectra.

On the other hand, new open-source software was established and managed by Eder Martioli, called OPERA for an Open-source Pipeline for ESPaDOnS Reduction and Analysis. The biggest inspiration of adapting this automatic pipeline for OES is, that within lots of useful modules and scripts for automatic reduction, extraction and different analysis of spectrum, contains modules for straighten up tilted spectral lines.

Thus the results in Fig 8.3 are compatible with theory. This effect is more noticeable in near infra-red part of the spectrum. Although, that is only one advantage of this new tool. OPERA is in comparison with IRAF, let's say, more user friendly, considerably faster and more efficient in automatic creation of master calibration images, determination of statistical quantities for wavelength calibration as spectral resolution, number of matching lines, wavelength and radial velocity precision and calculation of heliocentric correction, radial velocity corrections. Moreover, the source codes and modules are written in more modern and accessible codes, more easy to understand. All modules are written in C, whereas the running codes in Python. On the other hand IRAF's native programming language is Subset Pre-Processor.

The most important and also difficult part of the this thesis and process of producing pipeline for OES is to create wavelength calibration template. It seems like easy task, but sorts of problems convinced us otherwise. Mainly, the principal of first wavelength solution was missing some parameters and was not producing right results. Eder Martioli, after many consultations, offered solution including manual identification of lines of the star computed with Lovis-Pepe Thorium-Argon atlas. Moreover, he added some adjustments to OPERA in order to take this solution as sufficient enough, for calculation of wavelength calibration. This method was tested on sample data from Petr Škoda and is fully described in Chapter 7 together with main information and standard reduction and

extraction procedures.

To verify this procedures, OPERA reduction is compared with well know reduction from IRAF. Final spectra from both tools are presented in Chapter 8. This chapter also includes spectra from tau Bootis observed with Iodine cell. Results shown in Figs. (3.4 and 8.14) agree with theory which assume the decrease of intensity in spectrum observed with Iodine cell. Short description of Iodine absorption cell is introduced within the section 3.1 including the main characteristics, scheme and parameters of OES. The whole Chapter 3 is dealing with an comparison of echelle spectrographs from each part of the world. Closer look is taken not only on OES, but on OPERA's home-base echelle spectrograph ESPaDOnS, too. The main differences between those two instruments are in the spectral resolution and in the transport of light from telescope to the spectrograph. The fact that the spectra resolution is much higher in case of ESPaDOnS is closely related to the second difference. The light from telescope is fiber-fed to the ESPaDOnS. For OES light travels through slit and by several mirrors fed to the spectroscope. Fiber for OES in coude focus would need to be around 20 m long, together with lower high resolution than for ESPaDOnS, the losses of signal would be more significant. Although, fiber-fed OES is highly discussed in Stellar Department. Hopefully, in near future more possibilities of different optical fiber will offer solution.

Essential application of high-resolution spectrographs is included in this thesis in the Chapter 4. More accurate the determination of the position and shapes of spectral lines is offering more precise measurements of radial velocity closely related to one of the leading topics in modern Astronomy, search of extra-solar planets. The main characteristics and detection methods are described.

Clearly, further research will need to be concentrated on normalization of spectra in OPERA. Two difficulties are raising up. First is related to properties of star exposed on OES. The astronomical research of Stellar Department is mostly concentrated on hot stars, whose lines can be broad (from rotation too) in such a degree, that they are considered to be part of the continuum. On the other hand, some standard star need to be observed in order to perform flux calibration. Moreover, the normalization of spectrum from IRAF did not show the best result, because of uncalibrated flux from OPERA, this topic was not included into this thesis. Doubtlessly, normalization is important for further analysis and better comparison of changes in spectral lines.

Appendix A

Gnuplot scripts

Several gnuplot scripts were written in order remain the structure of generated output plots and make the work more effective, too.

Scripts for OPERA outputs

For instance script `opera_bLyr.gnu` will produce output image of extracted spectrum from OPERA.

```
#Script opera_bLyr.gnu generates plot of extracted
  spectrum.

reset
unset key

set encoding utf8
set terminal pngcairo enhanced font 'Helvetica,12'
set output "opera_bLyr.png"
set title "The Spectra of {/Symbol b} Lyrae from OPERA."
  font "Helvetica, 14"
set xlabel "{/Symbol l} (nm)"
set ylabel "Intensity"
set key top box 7
plot "c201307040002.spc" u 5:9 w dots
```

Scripts for comparison

As a sample is chosen gnuplot script for `spectrum_bLyr.gnu`, which has an output the whole spectrum of β Lyrae and has following form:

```
#Gnuplot script "spectrum_bLyr" to generate output
  spectra
```

```

reset
unset key

set encoding utf8
set terminal pngcairo enhanced font 'Helvetica,12'
set output "spectrum_bLyr.png"
set xrange [350:850]
set title "The Spectrum of {/Symbol b} Lyrae." font "
    Helvetica, 14"
set xlabel "{/Symbol l} (nm)"
set ylabel "Intensity"
set key top center box 7
set key font "Helvetica,10"
plot "c201307040002.spc" u 5:9 t "spectrum from OPERA (
    red)" w d, "betaLyr.dat" u ($1/10):2 t "spectrum from
    IRAF (green)" w d

```

In case of Balmer serie of hydrogen, only one sample script for H α is introduced.

```

#Script "spectrumHa_bLyr.gnu" generates spectra in H
    alpha.
reset
unset key

```

```

set encoding utf8
set terminal pngcairo enhanced font 'Helvetica,12'
set output "spectrumHa_bLyr.png"
set xrange [654:658]
set title "The Spectrum of {/Symbol b} Lyrae: H{/Symbol a
    }." font "Helvetica, 14"
set xlabel "{/Symbol l} (nm)"
set ylabel "Intensity"
set key top box 7
set key left top font "Helvetica,10"
plot "c201307040002.spc" u 5:9 t "spectrum from OPERA" w
    l lt 1 lw 1 , "betaLyr.dat" u ($1/10):2 t "spectrum
    from IRAF" w l

```

Scripts for rest of the lines differs only in settings of output, xrange and as following:

```

set output "spectrumHb_bLyr.png"
set xrange [485:488]
set title "The Spectrum of {/Symbol b} Lyrae: H{/Symbol b
    }." font "Helvetica, 14"

```

Consequently, files after plot includes names of files from both OPERA and IRAF extractions, in order to compare them visually.

Appendix B

Ruby scripts

Ruby for 1D to ASCII

Ruby scripts used for converting ".fit" format to ".dat" format. First script produces set of lines, one to extract each order separately with `scopy`, that means one-dimensional files and with `wspectext` converts 1D files to ASCII format.

```
# iraf_commands.rb
(1..ARGV[0].to_i).each do |n|
  puts "scopy #{ARGV[1]}.fit[* ,#{n},1] ly#{n}"
  puts "wspectext ly#{n} ly#{n}.dat"
end
```

B.1 Ruby for final data file

Second simply looks at the each file with "ly*.dat" in current directory and extract lines of this file starting with 143 till the end.

```
#iraf$\_filter.rb
Dir['ly*.dat'].each do |file|
  lines = File.readlines(file)

  puts lines[142..-1]
end
```

Appendix C

Manuals

Last appendix contains printed versions of reduction summary for both OPERA and IRAF reduction. Those manuals, from Wikipedia portal of Stellar Department¹.

To this thesis is also attached DVD containing IRAF and OPERA manuals for installation and reduction, full set of final test products from OPERA, reduced data from OPERA and IRAF together with gnuplot scripts to generate input images and their comparison.

¹<https://stelweb.asu.cas.cz/wiki/index.php/OPERA>

Bibliography

- [1] Barnes, Stuart. The design and performance of high resolution echelle spectrographs in astronomy. *Doctoral Dissertations Canterbury*, 2004.
- [2] Carroll, Bradley W.A. Dale, A. Ostlie. An introduction to modern astrophysics. *Reading: Addison-Wesley Publishing Company*, 1996. 1327, A-65: I-26 s. ISBN 0201547309.
- [3] Close, L. M., K. B. Folette, J. R. Males, A. Puglisi, M. Xompero, D. Apai, J. Najita, A. J. Weinberger, K. Morzinski, et al. Discovery of H α emission from the close companion inside the gap of transitional Disk HD 142527. *The Astrophysical Journal*, 2014. 781(2): L30–.
- [4] Eyser, L., L. Rimoldini, B. Holl, P. North, S. Zucker, D. W. Evans, D. Pourbaix, S. T. Hodgkin, W. Thuillot, N. Mowlavi, B. Carry. The Gaia Mission, Binary Stars and Exoplanets, *Proceedings of a Conference: Living Together Planets, Host Stars and Binaries*, 2015. 15p. arXiv:1502.03829
- [5] Grossová, Romana. Observační aspekty supernov. *Bakalářská práce, Masarykova univerzita*, 2013.
- [6] Churchil, C.W. Introduction to Echelle Data Reduction Using the Image Reduction Analysis Facility: Emphasizing the Hamilton Echelle Spectrograph, 1995. *Lick Observatory Technical Report*, No.74.
- [7] Konacki, Maciej. Precision Radial Velocities of Double-lined Spectroscopic Binaries with an Iodine Absorption Cell. *The Astrophysical Journal*. 2005, 431–438. DOI: 10.1086/429880. ISSN 0004–637x.
- [8] Koubský, P., P. Mayer, J. Čáp, F. Žďárský, J. Zeman, L. Pína and Z. Melich. Ondřejov Echelle Spectrograph OES. *Publ. Astron. Inst. ASCR*, 2004. 92: 37-43.
- [9] Mayor, M. et al. Setting New Standards with HARPS. *The Messenger*, 2003. 114: 20-24 (2003).
- [10] Mason J.W. Exoplanets: detection, formation, properties, habitability. *Springer Science & Business Media*, 2007. 314 p.
- [11] Moutou, C., L. Maset, L. Seliez-Vandernotte and M.-E. Desrochers. *New from CFHT/ESPaDOnS Spectropolarimeter*, 2015 : 201-204.

- [12] Parry, Ian R. The Astronomical Uses of Optical Fibers. *Fiber Optics in Astronomy III*. ASP Conference Series. 1998, 1998(Vol. 152): 3-13.
- [13] Perruchot, S., Ian S. Mclean, Mark M. Casali, D. Kohler, F. Bouchy, Y. Richaud, P. Richaud, G. Moreaux, M. Merzougui, et al. The SOPHIE spectrograph: design and technical key-points for high throughput and high stability. *Proceedings of the SPIE "Astronomical Telescopes and Instrumentation 2008"*, 2008. DOI: 10.1117/12.787379.
- [14] Raskin, G., H. van Winckel, H. Hensberge, A. Jorissen, H. Lehmann, C. Waelkens, G. Avila, J.-P. de Cuyper, P. Degroote, et al. HERMES: a high-resolution fibre-fed spectrograph for the Mercator telescope. *Astronomy and Astrophysics*, 2011. 526: 12p. DOI: 10.1051/0004-
- [15] Pepe, F., P. Molaro, S. Cristiani and R. Rebolo, et. al. ESPRESSO: The next European exoplanet hunter. *Astronomische Nachrichten*, 2014. (335, No.1): 10-22.6361/201015435. ISBN 10.1051/0004-6361/201015435.
- [16] Shames, Peter a Doug Tody. A User's Introduction to the IRAF Command Language: Version 2.3. 1986, : 1-91.
- [17] Škoda, Petr, Jaroslav Honsa and Miroslav Šlechta. Spectroscopy with Ondřejov observatory 2-m telescope. *Publications of the Astronomical Institute of the Academy of Sciences of the Czech Republic*, 2002, 73 s. ISBN 8090248764.
- [18] Tahir Yaqoob. Exoplanets and alien solar systems. *New Earth Labs (Education and Outreach)*, 2011. ISBN 978-097-4168-920.
- [19] WAKO, Aoki. Data reduction of echelle spectra with IRAF. National Astronomical Observatory of Japan, 2016, : 1-34.

Online references:

- [20] OES - Ondřejovský ešletový spektrograf [online]. ŠLECHTA, Miroslav. Available on: <http://stelweb.asu.cas.cz/~slechta/OES/pro-ian/>
- [21] The Extrasolar Planet Encyclopaedia - Catalog Listing. The Extrasolar Planets Encyclopaedia [online]. Exoplanet TEAM, 1995, 2015-12-2. Available on: <http://exoplanet.eu/catalog/>
- [22] IRAF Image Reduction and Analysis Facility [online]. NOAO in Tuscon, Arizona, 1982. Available on: <http://iraf.noao.edu/>
- [23] IRAF Image Reduction and Analysis Facility, X11iraf package [online]. NOAO in Tuscon, Arizona, 1982. Available on: <http://iraf.noao.edu/x11iraf/>

- [24] ESPaDOnS: An Echelle SpectroPolarimetric Device for the Observation of Stars at CFHT: Data reduction software: Libre-ESpRIT. Hawaii: managed by Nadine Manset. Available on: http://www.cfht.hawaii.edu/Instruments/Spectroscopy/Espadons/Espadons_esprit.html
- [25] ESPaDOnS: An Echelle SpectroPolarimetric Device for the Observation of Stars at CFHT: Data reduction software: Libre-ESpRIT. Hawaii: managed by Nadine Manset. Available on: http://www.cfht.hawaii.edu/Instruments/Spectroscopy/Espadons/Espadons_description.html
- [26] ESPaDOnS: The high-resolution spectrograph. Jean-François Donati, Hawaii. Available on: <http://www.ast.obs-mip.fr/projets/espadons/espadons/spectro.html>
- [27] Thüringer Landessternwarte Tautenburg: Coudé Echelle Spectrograph [online]. Available on: <http://www.tls-tautenburg.de/TLS/index.php?id=58>
- [28] William Herschel Telescope: UES USERS' MANUAL [online]. Available on: http://www.ing.iac.es/Astronomy/observing/manuals/html_manuals/wht_instr/ues/ues_manual.html
- [29] OPERA-PIPELINE: Echelle Spectro-Polarimeter Reduction pipeline [online]. brought to you by Douglas Teeple. Available on: <http://sourceforge.net/projects/operapipeline/>
- [30] NASA's Heasarc-Software: CFITSIO - A FITS File Subroutine Library. Version cfitsio 3.340 [online]. Developed by: Dr. William D. Pence . Available on: <http://heasarc.gsfc.nasa.gov/FTP/software/fitsio/c/cfitsio3340.tar.gz>